Simone Bochner de Araujo

Slot Coating of Particle Suspension

DISSERTAÇÃO DE MESTRADO

DEPARTAMENTO DE ENGENHARIA MECÂNICA

Programa de Pós-Graduação em Engenharia Mecânica

Rio de Janeiro
July 2014

Pontifícia Universidade Católica
do Rio de Janeiro

Simone Bochner de Araujo

Slot Coating of Particle Suspension

DISSERTAÇÃO DE MESTRADO

Dissertation presented to the Programa de Pós-Graduação em Engenharia Mecânica of the Departamento de Engenharia Mecânica, PUC–Rio as partial fulfilment of the requirements for the degree of Mestre em Engenharia Mecânica.

Advisor: Prof. Marcio da Silveira Carvalho

Rio de Janeiro
July 2014

Pontifícia Universidade Católica
do Rio de Janeiro

Simone Bochner de Araujo

Slot Coating of Particle Suspension

Dissertation presented to the Programa de Pós-Graduação em Engenharia Mecânica of the Departamento de Engenharia Mecânica do Centro Técnico Científico da PUC-Rio, as partial fulfilment of the requirements for the degree of Mestre.

Prof. Marcio da Silveira Carvalho
Advisor
Pontifícia Universidade Católica do Rio de Janeiro – PUC-Rio

Prof. Luis Fernando Alzuguir Azevedo
Pontifícia Universidade Católica do Rio de Janeiro – PUC-Rio

Prof. Francisco Ricardo da Cunha
Universidade de Brasília – UnB

Prof. José Eugenio Leal
Coordinator of the Centro Técnico Científico
Pontifícia Universidade Católica do Rio de Janeiro

Rio de Janeiro, July 24^{th}, 2014.

Simone Bochner de Araujo

The author graduated in Mechanical Engineering at PUC-Rio on August 2012. Works at PUC-Rio since March 2012 where she develops softwares for CENPES/Petrobras.

Bibliographic data

Araujo, Simone Bochner

Slot Coating of Particle Suspension / Simone Bochner de Araujo; advisor: Marcio da Silveira Carvalho. — 2014.

v., 93 f: il. ; 29,7 cm

Dissertação (Mestrado em Engenharia Mecânica) - Pontifícia Universidade Católica do Rio de Janeiro, Rio de Janeiro, 2014.

Inclui bibliografia

1. Engenharia Mecânica - Dissertação. 2. Método dos Elementos Finitos. 3. Processo de Revestimento. 4. Suspensão de Partícula. 5. Transporte de partícula. 6. Escoamento de Marangoni. I. Carvalho, Marcio da Silveira. II. Pontifícia Universidade Católica do Rio de Janeiro. Departamento de Engenharia Mecânica.. III. Título.

CDD: 621

To my family

Acknowledgments

I would like to thank my advisor, Prof. Marcio Carvalho, who guided me through my master and without whom I would not have developed the present work. Besides, I would like to thank him for his ideas and help.

I would also like to thank my family and Arnaud for all the support and encouragement.

I do also extend my gratitude for all my co-workers at the *Laboratorio de Micro-hidrodinamica em Meios Porosos*, my friends and professors at PUC-Rio.

Finally, I thank CNPQ and the Department of Chemical Engineering of the University of Minnesota for the financial support.

Abstract

Araujo, Simone Bochner; Carvalho, Marcio da Silveira. **Slot Coating of Particle Suspension**. Rio de Janeiro, 2014. 93p. Master Dissertation — Department of Mechanical Engineering, Pontifícia Universidade Católica do Rio de Janeiro.

Slot coating is a common method in the manufacturing of a wide variety of products. It belongs to a a class of coating method known as *premetered coating*: in a steady state operation, the thickness of the coated liquid layer is set by the flow rate fed to the die and the speed of the substrate moving past, and is independent of other variables of the process. For many applications, the coating liquid is a particle suspension. The common simplified approach is to study the flow as Newtonian and evaluate its viscosity based on the average particle concentration. However, experimental data shows that particle distribution is in fact non-uniform in shear flows. Moreover, particle distribution along the film thickness during the coating process will affect the final film structure and consequently product performance. Hence, it is important to understand the fundamentals of coating process with particle suspension to better describe and predict the behavior of the flow and the particle distribution in the coated layer. The goal of the present work is to study different particle migration mechanisms in a suspension that may affect particle distribution in the coated film; such as diffusive mecanisms and sedimentation. The model presented takes into account the viscosity dependency on local particle concentration and surface-active particles, i.e. Marangoni effect. Two different approaches were used to study Marangoni flow. First, the bulk-interface transport is considered much faster than bulk diffusion such that the net flux is zero and surface concentration is equal bulk concentration. The second, more complete model, considers adsorption and desorption fluxes from the interface. The non-linear system of equations, with appropriate boundary conditions, is solved by Galerkin Finite Element Method and Newton's Method. The flow is two-dimensional and therefore two-dimensional elements are used to describe flow domain. Nonetheless, in order to evaluate particle concentration along the interface a one-dimensional element was created. The coupling between those two classes of elements is discussed. The results show that the particle distribution on the coated layer is a strong function of the film thickness and suspension properties, such as particle density and diffusion coefficients. The Marangoni flow associated with surface tension gradient due to particle concentration variation along the interface can change the recirculation pattern and particle concentration distribution. Furthermore, the results show that

particle adsorption and desorption from interface have a strong effect on the particle distribution.

Keywords

Finite Element Method. Slot coating. Particle Suspension. Particle Transport. Marangoni Flow.

Resumo

Araujo, Simone Bochner; Carvalho, Marcio da Silveira. **Processo de Revestimento com Suspensão de Partículas**. Rio de Janeiro, 2014. 93p. Dissertação de Mestrado — Departamento de Engenharia Mecânica, Pontifícia Universidade Católica do Rio de Janeiro.

O processo de revestimento por extrusão é um método muito utilizado na manufatura de diversos produtos. Ele pertence à uma classe de processos de revestimento chamada revestimento com vazão pré-fixada: para operações em regime permanente, a espessura da camada de líquido revestida é definida pela vazão na entrada do equipamento e pela velocidade do substrato. Para diversas aplicações, o líquido de revestimento é uma suspensão de partículas. A abordagem comumente usada é analisar o escoamento como se o fluido fosse Newtoniano, onde sua viscosidade é avaliada pela concentração média de partículas. Porém, dados experimentais mostram que a distribuição de partículas não é uniforme em escoamentos com cisalhamento. Além disso, a distribuição de partículas no filme após o processo de revestimento afetará a estrutura final do filme e, consequentemente, a qualidade final do produto. Portanto, é importante entender os fundamentos do processo de revestimento com suspensão de partículas para melhor descrever este processo e prever comportamentos desse escoamento. O objetivo do presente trabalho é estudar diferentes mecanismos de migração de partículas em suspensão que podem afetar a distribuição de partículas no filme revestido; como mecanismos de difusão e sedimentação. O modelo apresentado leva em consideração a dependência da viscosidade pela concentração local de partículas e o efeito de Marangoni. Dois modelos diferentes foram usados para estudar o escoamento de Marangoni. No primeiro, o transporte de partículas entre a superfície e o escoamento é considerado muito mais rápido que a difusão no escoamento de tal forma que o fluxo líquido é zero e a concentração de partículas ao longo da superfície é igual à concentração de partículas na região do escoamento próxima à superfície. No segundo, um modelo mais completo, os efeitos de adsorção e dessorção de partículas pela interface é considerado. O sistema final de equações é não-linear e, com as condições de contorno apropriadas, é resolvido pelo método de Galerkin em elementos finitos e pelo método de Newton. O escoamento é bi-dimensional e, portanto, elementos bi-dimensionais são utilizados para descrever o domínio do problema. Entretanto, para avaliar a concentração ao longo da superfície, foi necessário criar um elemento uni-dimensional. O acoplamento entre estas duas classes de elementos também é discutido. Os resultados mostram que a distribuição de partículas no filme revestido é uma forte função da espessura

do filme e das propriedades da suspensão, como a densidade das partículas e coeficientes de difusão. O escoamento de Marangoni pode afetar o padrão de recirculação e a distribuição de concentração de partículas. Além disso, os resultados mostram que a adsorção e dessorção de partículas na interface afetam fortemente a distribuição de partículas.

Palavras–chave

Método dos Elementos Finitos. Processo de Revestimento. Suspensão de Partícula. Transporte de partícula. Escoamento de Marangoni.

Contents

List of Figures

List of Tables

Nomenclature

Greek Symbols

β	Surface tension gradient
δ	Slip coefficient
η	Vertical direction in reference domain
μ	Viscosity
$\dot{\gamma}$	Shear rate
κ	Interface curvature
μ_s	Suspension viscosity
∇_S	Surface gradient operator
ϕ	Concentration field
ρ	Density
$\bar{\sigma}$	Reference surface tension
σ	Surface tension
θ_u	Upstream static contact angle
θ_{dyn}	Upstream dynamic contact angle
ξ	Horizontal direction in reference domain

Roman Symbols

a	Particle radius
b	Feed slot height
$\bar{c}$	Average particle concentration
c	Particle concentration
Ca	Capillary number
c_b	Particle concentration in the bulk
C_D	Drag coefficient
c_{inf}	Particle concentration that saturates the interface
c_{int}	Particle concentration along the interface
c_m	Maximum packing particle fraction
D	Particle diameter

D_η	Diffusive constant for reference domain in η-direction.
D_ξ	Diffusive constant for reference domain in ξ-direction.
E	Buoyancy force
F_y	Force in the y-direction
F_D	Drag force
G	Velocity gradient field
g	Gravity
h	Gap to thickness ratio
H_0	Gap between die and substrate
I	Identity matrix
j	Total particle migration from/to bulk to/from the interface
k	Particle Transport Constants Ratio
k_a	Adsorption effect constant
K_c	Shear rate gradient constant
k_d	Desorption effect constant
K_μ	Viscosity gradient constant
$\mathbf{N}$	Total flux of particle migration
N_c	Flux of particles due to shear rate gradient
N_μ	Flux of particles due to viscosity gradient
$\mathbf{n}_f$	Normal vector to liquid free surface
N'_S	Flux of particles due to sedimentation taking into account other particles presence
N_S	Flux of particles due to sedimentation
$\mathbf{n}_w$	Normal vector to the wall
P	Weight force
p	Pressure field
P_{atm}	Ambient pressure
Pe	Peclet number
P_{vac}	Vacuum pressure
$\dot{Q}$	Flow rate

R	Interface curvature
Re	Reynolds number
S	Sedimentation dimentionless parameter
S_t	Stanton number
t	Film thickness
t'	Time
$\mathbf{T}$	Stress tensor
$\mathbf{t}_f$	Tangential vector to liquid free surface
U	Settling velocity
u	Velocity component in the x-direction
$\mathbf{v}$	Flow velocity vector
V	Web velocity
v	Velocity component in the y-direction
Vol	Volume
x	Horizontal direction in physical domain.
X_d	Downstream static contact line position
x_d	Extreme outside point of the downstream slot die
y	Vertical direction in physical domain.

Subscripts

l	Liquid
$part$	Particle
s	Suspension

Nothing great was ever achieved without enthusiasm.

Ralph Waldo Emerson, *American Philosopher.*

1
Introduction

Coating process is widely used in the manufacturing of different kinds of products. These products comprehend, for example, adhesive tapes, magnetic tapes, disks and optical films. Besides, coating processes are applied in more modern technologies such as plasma displays and cell phones/smart phones displays. Coating processes also take place in unexpected fields. For instance, in food industry several products such as candies, cereal and chocolate require coating; which means not only a successful process but also a tasty one.

For some applications, the process does not require high precision. On the other hand, for diplays, films and others, one defect in the order of 1 μm may compromise the functionality of the product and the process as a whole. Therefore, for high-precision coating processes, it is important to understand the fundamentals of the process, and describe it with accurate models.

In the present chapter the basics of coating - more specifically the slot coating - process are presented. Besides that, the Newtonian flow approach for coating with particle suspensions is presented; which is quite limited given the peculiarities of a particle suspension. The characteristics of particle suspension is also discussed further in this chapter. Finally, the goals of this work are presented.

1.1
Coating process

To coat is to substitute the air in contact with a substrate by a continuous liquid layer. During a coating process, one or several liquid layers are deposited on a solid substrate; subsequently they are dried to form solid films that serve specific functions - Kistler and Schweizer (1997). The interior of many coatings and films has to have particular microstructure or nanostructure in order to function as intended, whether optically, photochemically, electronically, magnetically, or mechanically.

A simplified scheme of how this process occurs is presented in Figure 1.1. First, a solution is prepared. The solution must contain the components that are desired at the final film. Once this liquid is ready, it will be deposited

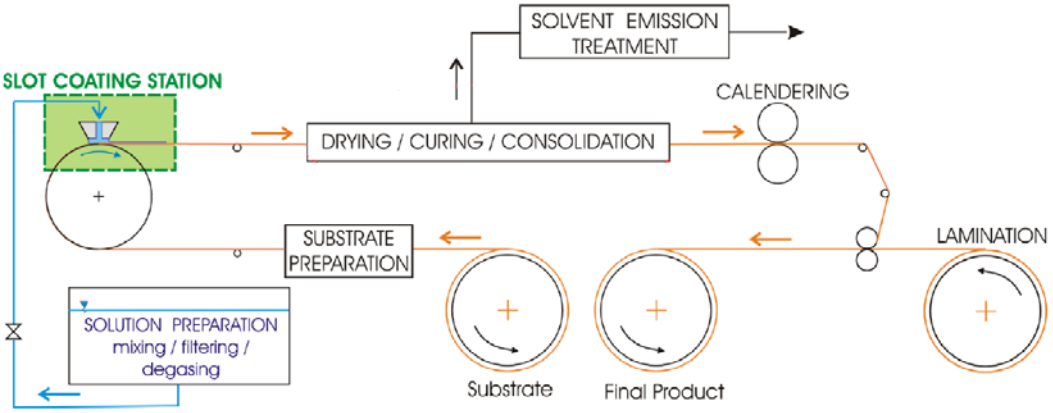

Figure 1.1: Scheme of a coating process.

on the web. There are many different kinds of coating processes, Figure 1.1 presents the slot coating; which will be the scope of our study. After, the process continues to the dryer where the film will be solidified. At the end of this last step, we have the final product.

To achieve the desired quality and functionality of a coating in an economical way, we must select the appropriate coating method. We can classify coating methods in several ways. Their most fundamental characteristic is the number of layers that can be applied per applicator. Single layer methods all apply one coating layer at a time and require several applicators in line to achieve the total number of layers necessary in the coating structure. Coating layers also can be distinguished by the uniformity of the coating and the inherent quality level that can be obtained (Cohen and Guroff (1992)). Some of these methods are presented below.

Dip Coating

Dip and brush coating are among the oldest coating methods. In dip coating, the continuous web, or an individual item, is dipped into the coating fluid and withdrawn from it. One or both sides of the web can be wetted. The fluid that adheres to the web determines the coating thickness, but scrapers or squeeze roll can remove excess material by a process known as doctoring. Fluid viscosity and density, coating speed, and angle of withdrawal determine the wet thickness before doctoring (Cohen and Guroff (1992)). A illustrative sketch of this process is shown in Figure 1.2.

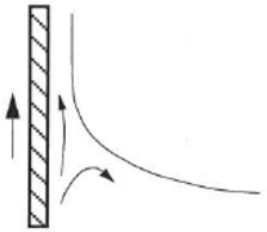

Figure 1.2: Dip coating process.

Knife Coating

Another coating process is the knife coating. In this process, a stationary, rigid knife doctors off the excess fluid. Knife coating fills in any depression in the support, giving a smooth coating surface. Figure 1.3 shows an example of knife over tensioned web where the knife is held against an unsupported web, and the depression of the knife and the web tension determine the force of the knife against the web.

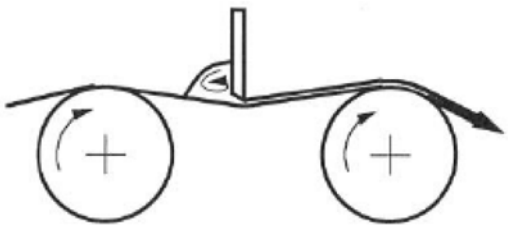

Figure 1.3: Knife coating over tensioned web.

Forward and Reverse Roll Coating

In forward roll coating, the applicator roll rotates in the same direction as the web, which is supported by an impression roll. Both the applicator roll and the web carry coating fluid beyond the nip, or region of closest contact and minimum clearance in the applicator. The amount of fluid the web picks up depends on the amount brought to the nip and the nature of film splitting beyond it. In reverse roll coating, the applicator roll rotates in the direction counter to the movement of the web on the impression roll. The amount of fluid the applicator roll carries to the nip is a factor of great interest because essentially all the fluid carried by the applicator roll is wiped off and picked up by the web moving in the reverse direction. A counterrotating metering roll often controls the amount carried by the applicator roll. Figure 1.4 shows a scheme of these processes.

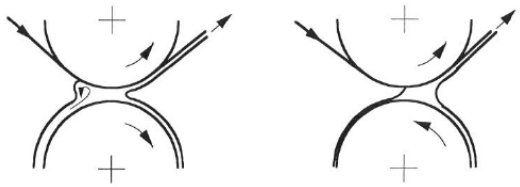

Figure 1.4: Forward and Reverse Roll Coating process.

Curtain Coating

In this method, a curtain of solution - formed by fluid overflowing a weir or passing through an extruder pointing downward - falls onto the moving web. This method was converted to a multilayer technique and adapted for multilayer photographic films by Kodac in the 1970s (Cohen and Guroff (1992)). Figure 1.5 presents a scheme of a multilayer curtain process.

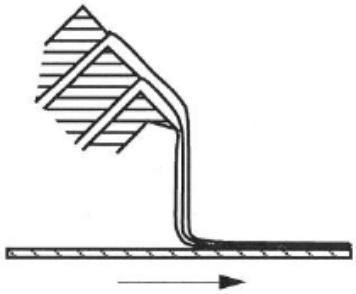

Figure 1.5: Curtain Coating process.

The last kind of coating process presented is the slot coating. As the slot coating process is the one that will be analysed in the present work, it will be presented more detailed in the next subsection.

1.1.1 Slot Coating

Slot coating belongs to a class of coating method known as premetered coating, in which all the fluid fed to the coating head is applied to the web (Cohen and Guroff (1992)). As a consequence, in a steady-state operation, the thickness of the coated liquid layer is set by the flow rate fed to the die and the speed of the substrate moving past, and is independent of other process variables. Thus, premetered methods are ideal for high-precision coating (Romero and Carvalho (2008)). However, the liquid flow in the application region (coating bead), and therefore the quality of the coated film, is strongly affected by operating parameters such as web speed, liquid properties, and the geometry of the die (Carvalho and Kheshgi (2000)).

In slot coaters, the coating fluid is forced out of a slot formed by two metal plates held close to the web, as shown in Figure 1.6. The channel is held very close to the web and fluid exiting from the slot forms a coating bead and is carried off by the web. The coating gap is the distance between the coating head and the web (Cohen and Guroff (1992)). The liquid in the gap, bounded upstream and downstream by gas-liquid interfaces, or menisci, forms the coating bead. In order to sustain the coating bead at higher substrate speeds, vacuum is usually applied to the gas upstream from the upstream meniscus (Carvalho and Kheshgi (2000)). The vacuum also permits thinner coatings.

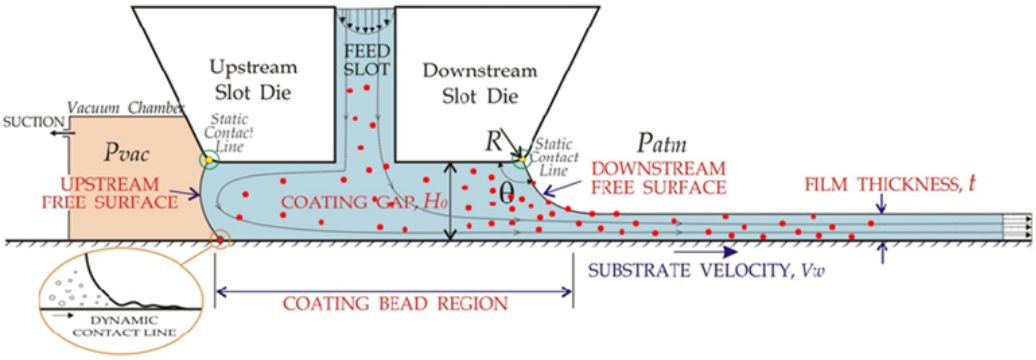

Figure 1.6: Scheme of the slot coating process.

The competiton among viscous, capillary and pressure forces, and, in some cases, inertial and elastic forces, sets the range of operating parameters in which the viscous free surface flow of the liquid can be two-dimensional and steady, which is the desired rate. The region in the space of operating parameters of a coating process where the delivered liquid layer is adequately uniform is usually referred to as a *coating window*. Knowledge of coating windows of different coating methods is needed in order to predict whether a particular method can be used to coat a given substrate at a prescribed production rate (Romero and Carvalho (2008)).

Most past analysis of slot coating flow have dealt solely with Newtonian liquids. Some of these analysis are presented in the next section.

1.2 Newtonian flow model

Some contributions about Newtonian flows are Ruschak (1976), Higgins and Scriven (1979) and Carvalho and Kheshgi (2000). They studied flow limits for given substrate speed, different viscosities and properties of the liquid. For example, they show that when liquid viscosity is low the most important boundary of the coating window is the *low flow limit*: the minimum

thickness of liquid that can be deposited from a gap of specified clearance at a given substrate speed. It was found that the minimum thickness that can be coated rises as the web speed increases, i. e. thin liquid layers can be deposited only at low web speed.

However, coating liquids in practice are polymer solutions or colloidal suspensions, or both. The common simplified approach is to study the flow as Newtonian and evaluate its viscosity based on the average behavior of the liquid. For instance, Schunk and Scriven (1990) proposed a constitutive equation to model mixed extension and shear in polymer solution processing by using a generalized Newtonian model in which the liquid viscosity is an arithmetic average of the shear viscosity and the uniaxial extensional viscosity. Later, Romero et al. (2004) also used this model to study the low-flow limit in slot coating of an extensional thickening polymer solution. The results of this work were also compared with experiments done by the authors.

The Newtonian flow approach for particle suspensions where the liquid is assumed Newtonian and its viscosity is based on the average particle concentration was found to be not reliable as experimental data showed that the particle distribution is non-uniform in shear flows, such as presented by Leighton and Acrivos (1987). Therefore, it is important to study the fundamentals of a coating process with particle suspension to better describe and predict the behave of this flow. In order to do so we must take into account particle migration mechanisms due to particle interaction during the flow.

1.3 Coating of particle suspension

Suspension of particles in a liquid medium are ubiquitous. Blood, paint, ink, and cement are examples that hint at the diversity and technological importance of suspensions. Control of the structure and flow properties of such suspensions is often vital to the commercial success of the product or of its manufacture (Larson (1999)). Often unnoticed by the consumer, they make everyday objects scratch resistant, less reflective, colorful, or hydrophobic. Although the chemistry of these coatings is important, oftentimes their microstructure is just as influential in determining overall functionality. For example, the arrangement of carbon particles in a fuel cell electrode determines the permeability of the coating to reactive hydrogen and oxygen as well as the conductivity of the electrode. The required microstructure that makes these coatings functional develops as the dispersion of particulates suspended in a liquid is deposited and later dries into a solid film (Cardinal et al. (2010)). Concentration gradients in a drying coating process often lead to property variations along the film

thickness of the final product and can also influence particle arrangement and packing. Concentration gradients may be undesirable, but they may also be beneficial; such as in the design of layered microstructures in coatings containing more than one type of particle. Therefore, it is crutial to understand and predict the particle distribution in the film before it gets to the dryer. The particle arrangement will directly affect the drying process and, as a consequence, the product performance.

Previous analysis of particle suspension drying process such as the one presented in Cardinal et al. (2010) considers that the particle distribution will be uniform after the coating process. However, experimental data, such as those presented by Leighton and Acrivos (1987), show that shear flows induce migration of particles in concentrated suspension; thus particles are not uniformly distributed along the film thichness. Therefore, the flow over a slot coating process will present several different characteristics that can induce particle migration and, as a consequence, make the particle distribution at the coated film non-uniform.

One of the consequences of this non-uniformity is the presence of particle agglomeration in the flow. Another study such as Apostolou and Hrymak (2008) analysed the agglomeration process in coating geometries. In that study, the particles are assumed spherical in shape and the fluid phase is considered Newtonian and incompressible. The approach was quite limited since it is a one-way coupling: the fluid affects the motion of the particles, but the particles do not have any effect on the behavior of the flow. To justify this approximation they consider the density of the particles closer to that of the fluid and that the size of the particles is small relative to the flow dimensions. Still, this assumption is violated when the particles agglomerate forming larger structures or when they deposit on the flow boundaries forming obtructions to the flow.

More recent works follows a more complete two-way coupling, where not only the flow affects the motion of particles but particles also affect the flow. For instance, Min and Kim (2010) simulated particle migration for two different free-surface flows: a two-dimensional jet flow and a slot coating. In that study the particles suspended in a Newtonian fluid are neutrally buoyant, and the radii of the particles are the same. Besides, the particle size is large enough to neglect Brownian diffusion, but small enough to regard the suspension as a continuum and to neglect the wall effect. In order to describe the particle migration the model proposed by Phillips et al. (1992) is used and Krieger (1992) model is used to describe how the viscosity varies with particle concentration. The results show that even though the velocity profile

is fully developed and becomes flat, the particle distribution does not reach an uniform distribution in both cases. Therefore, we may not assume that particle concentration profile will be only a function of the velocity profile as done previously by Apostolou and Hrymak (2008).

Nonetheless, there are other flow parameters that may change the final particle distribution, such as the final film thickness. Silva and Carvalho (2013) studied the influence of film thickness on the final particle distribution. The hyphotesis that they used were similar to those described above, used in Min and Kim (2010) work. It was found that the final particle distribution is indeed a strong function of the film thickness. Depending on the final film thickness, the particle profile may present higher concentration at the top or at the middle of the coated film. This happens because the flow under the downstream die changes accordingly to the film thickness and, as a consequence, the effects of migration mechanisms will also vary, resulting in different particle profile configurations.

The aforementioned particle migration mechanisms, Phillips et al. (1992) proposed that particle migration is driven by shear rate gradient and viscosity gradient, not to mention Brownian diffusion. Yet, the relative contribution of these migration mechanisms on the final particle profile has not been studied. The present work studies the influence of this and others aspects of the coating process on the final particle concentration profile and flow pattern in the coating bead. The scope of the work is presented in the next section.

1.4 Scope of the work

As mentioned before, particle distribution at the coated film is extremely important for product performance. As a consequence, the goal of the present work is to study the different mechanisms that may affect particle distribution in the coated film; such as diffusive mechanisms and sedimentation.

Particle distribution may also affect the surface tension at the interface. Another objective of our work is to study the influence of surface tension gradient in the final particle distribution. In order to include this effect we will consider not only that the surface tension is a function of the particle concentration in the surface, but also that there might be particle transport from the bulk to the interface and vice-versa.

The next four chapters present the work developed. In Chapter 2, the mathematical formulation is presented; including the hyphotesis used and the equations of momentum conservation, mass conservation and particle tranport. In this chapter some dimentionless parameters are also defined in order to

analyse the relative contribution of different migration mechanisms on the final particle distribution. Chapter 3 describes the solution method used to solve the two-dimensional, steady-state free surface flow with particle suspension. To solve that we use finite element and Newton's methods. Besides, it also presents the characteristics of each element created - 1D and 2D elements - and the coupling between those two elements to solve the problem. Chapter 4 presents a qualitative flow analysis of the process, which describes some flow conditions and most relevants migration mechanisms in each area of a coating flow. Chapter 5 shows the results found for the particle distribution along the final film and the resulting flow pattern as a function of the dimentionless parameters defined in Chapter 2. Finally, Chapter 5 sumarizes the conclusions that were achieved through the study.

2
Mathematical Formulation

Flows with particle suspensions behave differently from a simple liquid flow with constant viscosity. The configuration of the flow in coating process is extremely important due to the required precision. Therefore, it is important to understand and comprehend the fundamentals of the coating process in order to predict and better model this process. This is also essential for the optimization of the process.

In this Chapter, the mathematical formulation is presented; which concerns the mass and momentum conservation equations, the particle transport equation and description of different particle migration mechanisms, boundary conditions, and equations to evaluate the liquid properties as a function of local particle concentration. Two approaches were considered to evaluate the dependency of surface tension with particle concentration along the interface. The first one considers that bulk-interface transport is much faster than bulk diffusion, such that the net flux is zero and surface concentration is equal bulk concentration. The second one considers adsorption and dissorption fluxes from the interface. Moreover, constitutive equations were used to describe the three migration mechanisms considered in this work: shear rate gradient effect, viscosity gradient effect and sedimentation. Finally, some dimentionless parameters are introduced in order to study the final particle distribution in the film as a function of the relative contribution of one transport mechanism with respect to another.

2.1
Geometry

The cross section of the geometry of slot coating process is shown in Figure 2.1. This process is ideally two-dimensional and in steady state in order to obtain a uniform film thickness in the downweb and crossweb directions.

From Figure 2.1 we have that:

- the final final film thickness is t $[mm]$;
- the gap between the dies and the substrate is H_0 $[mm]$;
- the substrate moves with a constant velocity V $[mm/s]$;

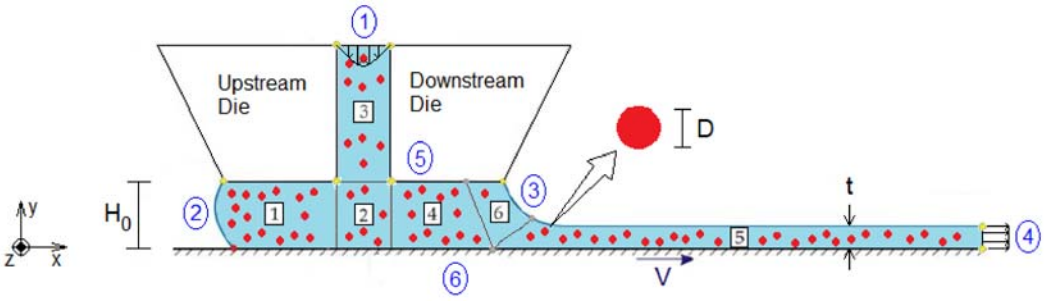

Figure 2.1: Geometry of the problem with the indication of some variables.

– the particles are spherical and its diameter is D $[mm]$.

Besides that, other important parameters are:

– the flow rate $\dot{Q}$ $[mm^3/s]$ -> which enters at boundary ①;
– the vacuum pressure P_{vac} $[Pa]$ -> which acts at boundary ②;
– the atmosferic pressure P_{atm} $[Pa]$ -> which acts at boundary ③.

The boundaries of the flow are shown in figure 2.1. Each of the boundaries have specific characteristics, such as:

1. Feedslot entrance: The liquid pumped in the feedslot is considered developed and the particle concentration distribution is uniform at this point.
2. Upstream free surface: The curvature and the position of this free surface is unknown and one of the variables of the problem; which will be a function of the pressure difference between the vacuum pressure from the vacuum chamber and the pressure in the fluid. The curvature of this free surface will also depends on the contact angle between the subtrate and the liquid. For coating process, the liquid usually wets the surface.
3. Downstream free surface: Similar to the upstream free surface, however the curvature and position of this free surface is a function of the pressure difference between the ambient pressure and fluid pressure.
4. Final film: The flow is also considered developed here. The particle concentration distribution will be determined after solving the problem.
5. Die wall: The non-slip and no-penetration conditions are applied along the die surface.
6. Substrate: The liquid moves with the same velocity of the substrate, except at the dynamic contact line.

As mentioned, the present problem presents two free surfaces which shall be determined. As a consequence, the flow domain is unkown a priori and is one of the variables of the problem. We want to determine the velocity, pressure and the particle concentration fields. Hence, the variables of the problem are:

- (x, y) -> Flow domain
- $u(x, y)$ -> velocity component in the x-direction
- $v(x, y)$ -> velocity component in the y-direction
- $p(x, y)$ -> pressure field
- $c(x, y)$ -> particle concentration distribution

The solution method to deal with the free boundary problem is discussed in detail in Chapter 3.

To determine velocity, pressure and particle concentration profiles, equations for the momentum conservation, mass conservation and particle migration mechanisms are used. These equations are discussed in the following sections. Before that, some of the hypothesis that were used are:

1. Steady state flow.
2. Stoke's flow.
3. Incompressible liquid phase.
4. Newtonian flow.
5. Two-dimensional flow.
6. Non-colloidal suspension.
7. Spherical and rigid particles.
8. Neglect inertial effects.
9. Rigid slot dies and substrate.
10. No sources and/or sinks of particles in the suspension flow.

The forth hypothesis states that the flow is Newtonian. This means that the fluid viscosity does not change with shear rate. However, it may change with particle concentration (this matter will be further discussed in section 2.3.2). Besides, we consider that the fluid density is constant.

2.2 Mass and Momentum Conservation

In order to determine velocity and pressure fields we use mass and momentum conservation equations. The mass conservation equation is shown in equation 2.1.

$$\frac{\partial \rho}{\partial t'} + \nabla \cdot (\rho \mathbf{v}) = 0 \tag{2.1}$$

However, one of the assumptions of this study is that the flow is under the steady state regime and that the liquid is incompressible. Therefore, we can simplify equation 2.1 to:

$$\nabla \cdot \mathbf{v} = 0 \tag{2.2}$$

For the momentum conservation equation and Stoke's flow, we have:

$$\nabla \cdot \left[-p\mathbf{I} + \mu\left(c\right) \left(\nabla \mathbf{v} + \left(\nabla \mathbf{v} \right)^T \right) \right] = 0 \tag{2.3}$$

The liquid viscosity is assumed to be a function of the local particle concentration.

2.3 Concentration Field

As mentioned earlier, particle distribution in the final film is crucial for the performance and functionality of the coated layer. Therefore, an accurate model to describe how particles suspended in a liquid are transported is necessary.

A simple particle mass balance leads to a convective-diffusive equation that describes the particle volumetric concentration field c:

$$\mathbf{v} \cdot \nabla c + \nabla \cdot \mathbf{N} = 0, \tag{2.4}$$

where $\mathbf{N}$ is the total particle flux, that is directly related to the different forces acting on the particles. Here, we consider non-colloidal suspensions, e.g., the particle radius is larger then 1 μm. The particle Reynolds number is very small and inertial forces can be neglected.

For small enough particles (radius < 1 μm), Brownian forces acting on the suspended particles usually leads to a homogeneous suspension, at which the particle concentration is constant (Fick diffusion).

However, if particles diameter is large enough, Brownian forces are negligible compared to other forces.

Numerous experiments have measured and reported that particles in an initially homogeneous suspension migrate towards the lower shear rate regions in a shear flow (Gadala-Maria and Acrivos (1980)). Because the particle Reynolds number is very small, inertial effects cannot explain the observed phenomena. Moreover, because the particles are large enough to make Brownian forces weak, the observed particle migration cannot be explained by suspending liquid-particle interaction. For non-colloidal suspensions, particle-particle interaction leads to particle transport in a shear flow.

Leighton and Acrivos (1987) have proposed a mecanism for particle transport based on particle-particle interaction frequency and effective viscosity of the fluid.

A simplified model is used to describe this total flux of particles by three different mechanisms. In the following sub-sections these three migration mechanisms are presented. The first mechanism is due to shear rate gradient in the flow. The second mechanism is due to viscosity difference in the flow. Finally, the third mechanism is due to gravity and density difference between the particles and the liquid, in other words, sedimentation.

2.3.1 Shear Rate Gradient Migration Mechanism

The shear rate is intimately related to the particle collision frequency. Areas with high shear rate present higher collision frequency than areas with low shear rate. In order to understand the overall behavior, a two-body collision analysis is made.

It is convenient to think of a shear flow as an assemblage of shearing surfaces sliding relative to one another. A diagram of an irreversible two-body collision in a constant shear rate flow is shown in Figure 2.2(a). A collision such as that shown in Figure 2.2(b) occurs when two particles embedded in adjacent shearing surfaces with different velocity move past one another. Since these collisions can cause a particle to be irreversibly moved from its original streamline, a particle which experiences a higher frequency of collisions from one direction than from the opposing direction will migrate normal to its shearing surface and in the direction of the lower collision frequency (Phillips et al. (1992)). As a consequence, particles migrate from high to low shear rate regions.

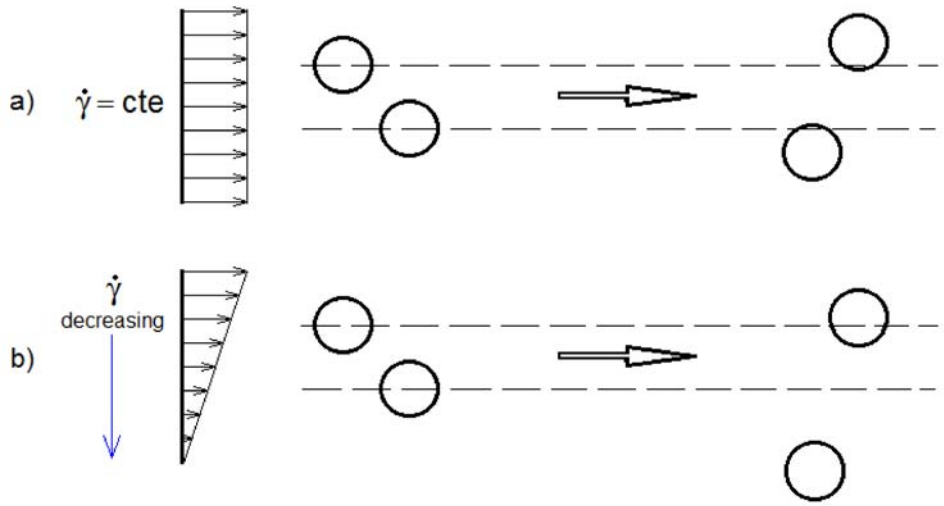

Figure 2.2: Schematic diagrams for an irreversible two-body particle collision with (a) constant shear rate flow and (b) not constant shear rate flow.

The constitutive equation used in this work to describe this mechanism

is the one proposed by Phillips et al. (1992), which is a modified version of Leighton and Acrivos (1987)' flux expression; it states that the flux N_c caused by the effect of spatially varying interaction frequency is a function of the local shear rate, the local particle concentration, the particle radius and a proportionality constant. The expression is given by

$$N_c = -K_c\, a^2 \left(c^2\, \nabla\dot{\gamma} + c\, \dot{\gamma}\nabla c\right) \tag{2.5}$$

where K_c is a proportionality constant of order unity that is found from experimental data. As the goal of this work is not experimental, the results will be shown as a function of this constant. In other words, we study the particle distribution for different values of K_c.

2.3.2 Viscosity Gradient Migration Mechanism

Another effect to be considered is given by the existence of gradients in the particle concentration or spatially varying viscosity $\mu(c)$.

Consider a single marked sphere of radius a in a suspension of otherwise identical spheres undergoing a viscous linear shear flow $u = \dot{\gamma}y$, where u is the velocity in the x-direction. As the sphere interacts with its neighbours in the shear flow, it will experience a series of displacements in y-direction with a characteristic length proportional to a and a frequency proportional to the shear rate $\dot{\gamma}$. In the absence of any gradient in concentration, these displacements will be random with zero mean (i.e. on average the particle will remain on its initial streamline), and thus will constitute a random walk. But in the presence of a concentration gradient such a random walk will lead to a diffusive flux and thus may be characterized by a diffusion coefficient, in this case with the dimensional scaling $\dot{\gamma}a^2$. It is important to note that in a dilute suspension the spheres will return to their initial streamlines at the end of all two-particles interactions owing to the linearity of the viscous-flow equations when only viscous forces are present. As a consequence, at least three particles must interact to yield the permanent displacements that lead to a random walk, and therefore, since the rate at which two particles interact with the marked sphere is proportional to $\dot{\gamma}\phi^2$, the diffusion coefficient must be proportional to $\phi^2\dot{\gamma}a^2$ in the dilute limit (Leighton and Acrivos (1987)).

Interparticle interactions in the presence of a gradient in concentration lead to an average displacement of the marked sphere from regions of high to low concentration.

From another point of view, high particle concentration areas yields high viscosity areas. The areas with high viscosity also present higher resistance

to motion when compared to low viscosity areas. Therefore, there will be a particle flux from high to low viscosity areas (high to low concentration areas), where the particles may flow more freely.

Figure 2.3 shows a scheme of two different kinds of two-body flow collisions: the first one for a constant viscosity flow and the second one for a non-uniform viscosity flow.

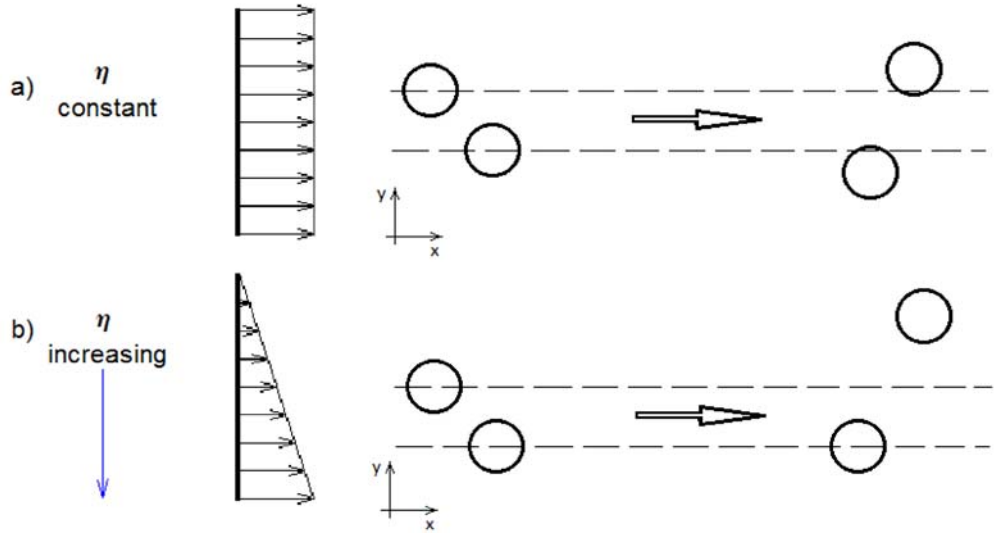

Figure 2.3: Schematic diagram for an irreversible two-body particle collision with (a) constant viscosity and (b) spatially varying viscosity.

As shown in the figure 2.3(a), for a constant viscosity flow particles are symmetrically displaced away from its collision point. On the other hand, if the viscosity is not uniform, figure 2.3(b), spheres are displaced in the direction of the lower viscosity area. The expression used to quantify this flux is also the one proposed by Phillips et al. (1992) which is a modified version of Leighton and Acrivos (1987)' flux expression and is presented in equation 2.6.

$$N_\mu = -K_\mu \, \dot{\gamma} \, c^2 \left(\frac{a^2}{\mu}\right) \frac{d\mu}{dc} \nabla c \tag{2.6}$$

Where N_μ is the particle flux due to the spatial variation in the viscosity and K_μ is a rate constant of order unity. The same analysis to the shear rate constant will be done here. Instead of experimentally determine the value of K_μ, we will study the possible outcomes of the particle distribution given different values of K_μ.

In this work instead of considering a constant viscosity for the concentrated suspension flow, an empirical viscosity model proposed by Krieger (1992) was used to describe it. Krieger (1992) proposes an expression that permits predicting the steady-state viscosity of a uniform hard-sphere

suspension of any diameter in a medium of any viscosity, as a function of the particle volume fraction. The simplified expression used in this work is then given by:

$$\mu_s = \mu \left(1 - \frac{c}{c_m}\right)^{-1.82}, \tag{2.7}$$

where c_m is the maximum packing fraction, considered here as $c_m = 0.68$. The maximum packing fraction represents the volume fraction for which the suspension viscosity tends to infinity.

The first mechanism - shear rate gradient - will tend to concentrate particles in the lower shear rate area, therefore the viscosity will increase in the lower shear rate area. On the other hand, the second mechanism - due to viscosity gradient - will act in the opposite direction of the first one; particles will flow away from higher viscosity areas. It is interesting to notice that this two mechanisms do opposed to one another. However, they do not necessarily compensate each other.

The last mechanism is independent of the flow and, as a consequence, is not correlated with the other two mechanisms.

2.3.3 Sedimentation

In many applications particles present higher density than the liquid where they are imersed in. The density difference will cause the sedimentation of the particles, which will affect the final particle distribution in the film. Consequently, it is also necessary to consider the migration mechanism due to gravity and density difference.

Figure 2.4 shows a scheme of the sedimentation process evolution by time.

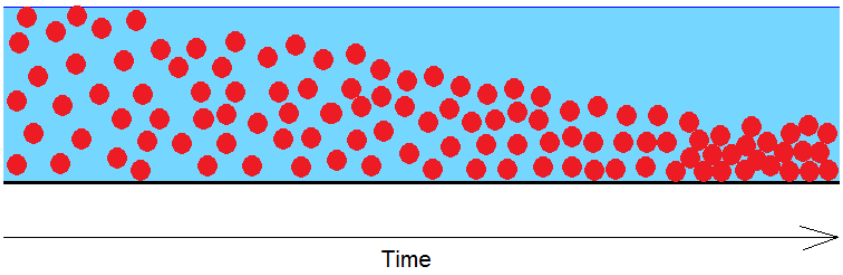

Figure 2.4: Sedimentation evolution by time.

In order to study the sedimentation mechanism, first it is necessary to evaluate the settling velocity. For a Stoke's flow around a sphere we have that the drag coefficient is given by:

$$C_D = \frac{24}{Re} \tag{2.8}$$

The force diagram during the settling motion is shown in Figure 2.5

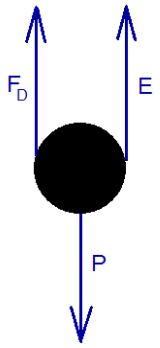

Figure 2.5: Diagram force for immersed particles.

Evaluating the sum of the forces acting in the y-direction, we have that:

$$\sum F_y = 0 \tag{2.9}$$

$$F_D + E - P = 0 \tag{2.10}$$

Each term of equation 2.10 can be expanded as:

$$E = \rho_l \; g \; Vol = \rho_l \; g \left(\frac{4}{3}\pi \; a^3\right) \tag{2.11}$$

$$P = \rho_{part} \; g \; Vol = \rho_{part} \; g \left(\frac{4}{3}\pi \; a^3\right) \tag{2.12}$$

$$F_D = \frac{C_D}{2}\rho_l \; U^2 \; \pi \; a^2 = \frac{24}{Re}\frac{\rho_l \; U^2 \; \pi \; a^2}{2} = 6\mu_l \; U \; \pi \; a \tag{2.13}$$

Subsituting the expressions in equations 2.11, 2.12 and 2.13 in equation 2.10, we find that the settling velocity is given by

$$U = \frac{2}{9}\frac{\Delta\rho \; g \; a^2}{\mu_l} \tag{2.14}$$

where $\Delta\rho$ is the density difference between the particle and the liquid ($\rho_{part} - \rho_l$).

The particle flux due to sedimentation will be a function of both settling velocity and of the particle concentration:

$$N_S = U \cdot c \tag{2.15}$$

As we have a flow with multiple particles, it is necessary to consider that each particle movement may be influenced by the particle concentration nearby. Thus, a correction factor to equation 2.15 is taken into account in order to consider the presence of other particles (Miskin et al. (1996)). The final equation that describes the flux of particles due to sedimentation is given by:

$$N'_S = \frac{2}{9}\frac{\Delta\rho\ g\ a^2}{\mu_l} c \frac{1-c}{\mu_s} \tag{2.16}$$

where μ_s stands for the suspension viscosity.

2.4 Boundary Conditions

As shown in Figure 2.1 there are six boundaries along which we must define conditions for. Boundaries ① and ④ are artificial boundaries where we just state that the flow is developed. The boundaries ② and ③, on the other hand, are liquid-air interface, where force balance and particle flux must be inforced. In this section are presented boundary conditions for the momentum conservation and particle transport equations for each of the six boundaries. To help the reader, figure 2.1 is re-presented in figure 2.6.

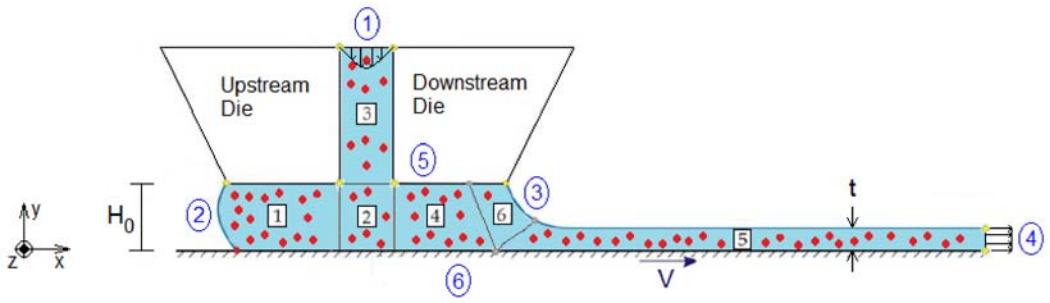

Figure 2.6: Geometry of the problem with the indication of boundary conditions.

① At the inflow plane, that is, at the die feeding slot, fully developed parallel rectilinear flow is assumed, where a Couette-Poiseuille velocity profile is prescribed as a function of the flow rate:

$$\begin{aligned} u &= 0 \\ v &= -\frac{6\,\dot{Q}}{b}\left[\left(\frac{x}{b}\right) - \left(\frac{x}{b}\right)^2\right] \end{aligned} \tag{2.17}$$

Where b is the feed slot height.

② At free surfaces, the traction in the liquid balances the capillary pressure and there is no mass flow rate across the gas-liquid interface. It is assumed that the gas viscosity is much smaller that the liquid viscosity, leading to vanishing shear stress along gas-liquid interface:

$$\mathbf{n}_f \cdot \mathbf{T} = \sigma\left(c_{int}\right)\kappa\mathbf{n}_f + \nabla_s\sigma\left(c_{int}\right)\mathbf{t}_f \tag{2.18}$$

And the kinetic condition for steady state flow is:

$$\mathbf{n}_f \cdot \mathbf{v} = 0 \tag{2.19}$$

The upstream static contact line is free to slide along the upstream die face at $y = H_0$ with a specified upstream static contact angle, θ_u. The mathematical condition is:

$$\mathbf{n}_w \cdot \mathbf{n}_f = \cos(\theta_u), \tag{2.20}$$

where n_w is the normal vector to the wall and n_f is the normal vector to free surface.

At the web surface the liquid translates with the web except near the locations where the liquid first appears to contact the web. This sub-microscopic region is called the dynamic contact line. In this short region, the Navier slip boundary condition makes the flux of momentum tangential to the web proportional to the velocity discontinuity between liquid and web. Without the slip condition, there is a non-integrable singularity in shear stress. The contact angle θ_{dyn} between liquid-air interface and solid surface needs to be specified as a boundary condition:

$$\begin{aligned} &\delta\ \mathbf{t}_w \cdot (\mathbf{v} - V\mathbf{i}) = \mathbf{t}_w \cdot (\mathbf{n}_w \cdot \mathbf{T}) \\ &\mathbf{n}_w \cdot \mathbf{n}_f = \cos\left(\theta_{dyn}\right) \end{aligned} \tag{2.21}$$

Where δ is the slip coefficient.

Besides, there is no net particle migration from the bulk to the interface and vice-versa. The concetration along the surface is taken to be equal to bulk concentration:

$$n \cdot \mathbf{N} = 0 \tag{2.22}$$

③ Similar condition to the upstream free surface, however instead of vacuum pressure, the gas pressure is usually atmosferic. The pressure is used in

the calculus of the meniscus curvature.

The downstream static contact line, X_d, is pinned to the sharp edge of this die:

$$X_d = (x_d, H_0), \tag{2.23}$$

where x_d is the position of the extreme outside point of the downstream slot die.

Same condition as the upstream free surface, there is no net particle migration from the bulk to the interface and vice-versa.

④ At the outflow plane, the free boundary condition was used. The liquid traction was simply evaluated immediately upstream of the outflow plane from its representation in the finite element basis function set:

$$\mathbf{n}_f \cdot T = -p\mathbf{n}_f + \mathbf{n}_f \cdot \left[\nabla\mathbf{v} + (\nabla\mathbf{v})^T\right] \tag{2.24}$$

⑤ The no-slip and no-penetration conditions applies along the die walls:

$$\begin{aligned} u &= 0 \\ v &= 0 \end{aligned} \tag{2.25}$$

⑥ Along the moving substrate, the no-slip and no-penetration conditions are applied:

$$\begin{aligned} u &= V \\ v &= 0 \end{aligned} \tag{2.26}$$

The second and third boundary conditions are functions of surface tension; which, by the way, is a function of particle concentration along the interface. As a consequence, we need an equation to evaluate the surface tension as a function of the particle concentration along the interface. First, we consider that the net flux of particles from the bulk to the interface is zero, as both boundaries states. Therefore, surface particle concentration is the same as bulk concentration. Later this will be changed as is presented in next sections and particle migration from/towards the interface is considered and particle concentration along the interface is different from bulk concentration.

2.5 Marangoni Flow

The simplified continuum concept of an interface is a surface containing no mass but with continuous tangential velocity and temperature. Surface tension

acts within the interface and results in a pressure jump across a curved interface. Constant surface tension leads to continuity of the viscous shear stresses on either side of the interface (Panton (2005)).

Coating flows are of sufficiently small scale that cappilary forces are usually important. The surface tension of the liquid/air interface, σ, characterizes the magnitude of capillary forces. In fact, the surface tension supports a pressure difference across a curved meniscus, with the higher pressure on the concave side (Kistler and Schweizer (1997)). The Young-Laplace equation, equation 2.27, states the relationship between pressure difference, surface tension and interface curvature.

$$\Delta P = \frac{2\,\sigma}{R} \tag{2.27}$$

Therefore, surface tension is important in determining the shape of interfaces and in certain instances promoting the flow within the bulk phases. Marangoni flow is a term to indicate that a gradient in the surface tension is the driving force of the flow. The surface tension may vary because of electrical effects, because the interface has various concentrations of absorbed foreign molecules, or simply because of the temperature. A variation in surface tension along the surface is accompanied by a jump in the viscous shear stresses on either side of the interface. Flows produced by this effect are called *'Marangoni Flow'* (Panton (2005)).

As presented before, several different particle migration mechanisms will affect the particle distribution of the coated film. Consequently, the particle concentration along the the film will not be uniform and this will probably affect surface tension. In order to consider this behavior, we used a linear constitutive equation to describe the surface tension as a function of the particle concentration, given by equation 2.28.

$$\sigma = \bar{\sigma} - \beta \cdot (c - \bar{c}) \tag{2.28}$$

Where $\bar{\sigma}$ is the reference value for surface tension, when particle concentration equals average particle concentration ($\bar{c}$). And β is the constant that measures particles strength. The greater β is, greater is the effect of particle concentration on surface tension. The considered behave, where surface tension decrease as particle concentration increases, was verified experimentally by Okubo (1995).

In Chapter 5, where the results are presented, we analyse Marangoni contribution for two different models. The first one considers the particle concentration used in equation 2.28 as being the bulk concentration. However,

the particle concentration at the interface may not be the same as the bulk due to particle migration towards to/away from the interface. As a consequence, the second analysis takes into account migration mechanisms closer to the interface. This second model is presented in the following section.

2.6 Mass Balance at the Interface

The first, simpler model, considers the particle migration from/towards the interface instantaneous, the particle concentration along the interface is equal to bulk concentration. However, particle concentration along the interface may be not the same as bulk concentration. In fact, particle migration closer to the interface may be described by two effects: adsorption and desorption effects. The adsorption effect concerns the capacity of the interface to adsorb particles. The second effect - desorption effect - evaluates interface capacity of let particles migrate away from the interface.

A possible representation for the sorptive flux (j) at the interface is the Langmuir-type kinetic expression, which is (Campana and Saita (2006)):

$$j = k_a \cdot c_b \cdot (c_{inf} - c_{int}) - k_d \cdot c_{int} \tag{2.29}$$

Where c_b is bulk concentration, c_{inf} represents the particle concentration that saturates the interface, c_{int} is the interface particle concentration, and k_a and k_d are the adsorption and desorption effects constants, respectively.

In this section we will also have to change the hypothesis done previously in section 2.4, where we stated that there was no particle migration from the bulk to the interface (equation 2.22). In fact, the flux is equal to the net flux away and from the interface.

$$\mathbf{n}_f \cdot N = j \tag{2.30}$$

Along the interface, the surface concentration distribution is described by a convective transport equation.

$$\mathbf{v} \cdot \nabla_S \, c_{int} = j \tag{2.31}$$

2.7 Dimentionless Parameters

Some dimentionless parameters will be used during the parametric study of the problem, presented in Chapter 5. These parameters are important to study the particle concentration distribution as a function of the flow, liquid and

particle characteristics. We want to study the influence of both diffusive and convective migration mechanisms, and to do that we define three dimentionless parameters that compare: the convective transport with the shear rate gradient diffusion; the shear rate gradient diffusion with viscosity gradient diffusion; and sedimentation diffusion with convective transport. A more detailed explanation of those parameters are presented as follows:

1. Hydrodynamic Peclet number (Pe): The Peclet number is defined as a ratio between the convective transport and the diffusive transport. The convective transport can be described by the flow rate which, as presented in sub-section 1.1.1, for slot coating processes is only a function of the film thickness and the substrate velocity. For a more general approach, the gap is used instead of the film thickness. The diffusive transport is described by the spatially varying interaction frequency migration mechanism because this effect is a straight consequence of the shear flow, which is related to the substrate velocity, and is the driving force for initial particle migration. Therefore:

$$Pe = \frac{convective\ transport}{diffusive\ transport} = \frac{V\ H_0}{K_c\ a^2\ \frac{V}{H_0}} \tag{2.32}$$

The final Pe number is written as:

$$Pe = \frac{1}{K_c}\left(\frac{H_0}{a}\right)^2 \tag{2.33}$$

2. Particle Transport Constants Ratio (k): Both particle migration mechanisms - due to shear rate gradient and viscosity gradient - are a function of constants K_c and K_μ, respectively. The particles transport constant ratio is given by the ratio of this two constants and it represents the relative contribution of each mechanism.

$$k = \frac{K_c}{K_\mu} \tag{2.34}$$

3. Sedimentation number (S): The dimentionless number that correlates the convective particle transport and the particle transport due to sedimentation is defined as the Sedimentation number. In order to analyse that we take the ratio between the settling velocity and the substrate velocity. Therefore, the Sedimentation number is given by:

$$S = \frac{sedimentation}{convective\ transport} = \left(\frac{2}{9}\frac{\Delta\rho\ g\ a^2}{\mu_l}\right)\cdot\left(\frac{1}{V}\right) \tag{2.35}$$

The final Sedimentation number is given by:

$$S = \frac{2}{9}\frac{\Delta\rho\ g\ a^2}{\mu_l\ V} \tag{2.36}$$

4. Stanton number (S_t): For the analysis that includes surface migration we do also use a dimentionless parameter known as Stanton number; which is the ratio between the adsorption effect constant along the interface and convective velocity, which for the present case is the web velocity. This dimentionless parameter is defined as S_t and is shown in equation 2.37.

$$S_t = \frac{k_a}{V} \tag{2.37}$$

5. Capillary number (Ca): Represents the relative effect of viscous forces over surface tension acting across an interface. This dimentionless parameter is presented in equation 2.38. Both viscosity and surface tension, which are a function of particle concentration, are evaluated for the average particle concentration.

$$Ca = \frac{\mu V}{\sigma} \tag{2.38}$$

6. Gap to thickness ratio (h): The gap, H_0, is defined as the distance between the dies and the substrate. The final film thickness is represented by t. Finally, the gap to thickness ratio parameter is defined by the ratio between these two parameters, as presented in equation 2.39.

$$h = \frac{H_0}{t} \tag{2.39}$$

3
Solution Method

This Chapter presents the method used to solve the coupled system of partial differential equations that describe the coating process with particle suspension. This problem is a free boundary problem, which the position of the upstream and downstream meniscus are unknown a priori. Hence, the flow domain is part of the solution. The free boundary problem is solved by mapping the unknown physical domain to a reference domain. The governing equations together with the equation that describes the mapping were solved using Galerkin Finite Element Method and are presented in section 3.1. Section 3.2 presents a summary of the basis functions used for the general two-dimensional element used. Finally, section 3.3 presents the one-dimensional element implemented to evaluate particle concentration along the interface, and the coupling between the two elements (1D and 2D elements).

3.1
Free Boundary Problem

As mentioned earlier, this is a free surface problem at which the position of the domain (downstream and upstream meniscus) is unknown. In order to solve this, the physical domain is mapped to a fixed and reference domain where the problem is solved. The coordinates of this new system are ξ and η. The mapping between physical and fixed domain becames, as a consequence, one of the variables of the problem. Figure 3.1 sketches this mapping.

The problem is two-dimensional, therefore two additional equations are needed to determine flow domain position. These equations are the differential diffusive equations for the iso- lines ξ and η coordinates of the reference domain presented in equation 3.1.

$$\begin{aligned} \nabla \cdot (D_\eta \nabla \eta) &= 0 \\ \nabla \cdot (D_\xi \nabla \xi) &= 0 \end{aligned} \tag{3.1}$$

These equations guarantee the orthoganality between iso-lines. D_η and D_ξ are diffusive constants. In order to solve these equations it is necessary to

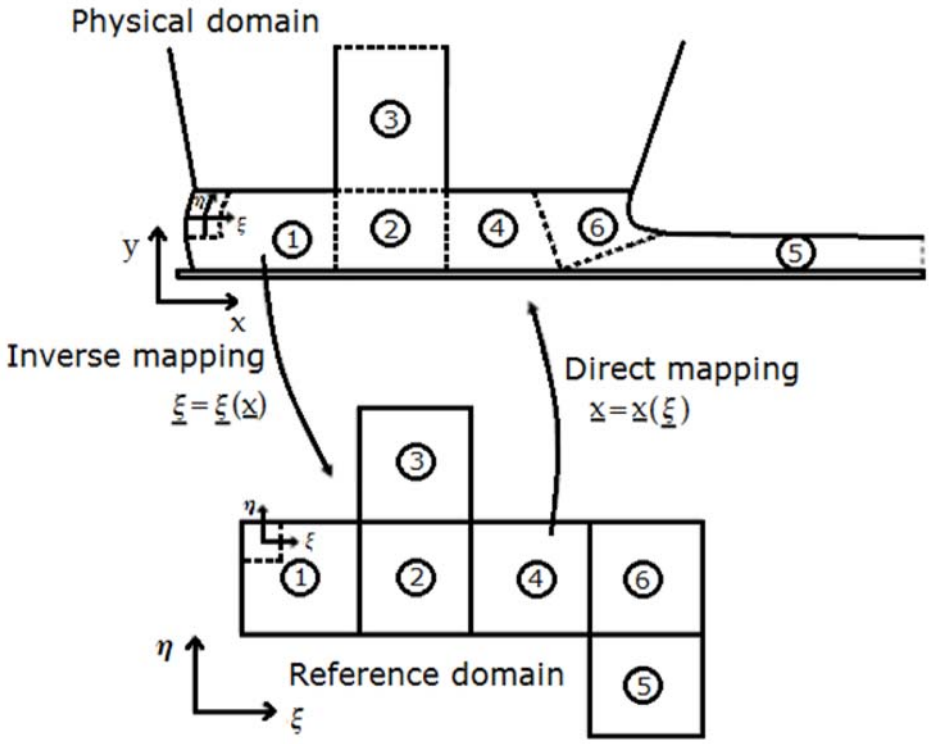

Figure 3.1: Scheme of the mapping between physical and reference domain.

define boundary conditions for the mapping. The complex domain is divided into quadrilateral regions. Figure 3.2 points out this sub-division and the boundaries of regions which are also boundaries of the problem.

Each region side needs two boundary conditions: one to specify the location of the boundary and another one to specify the distribution of the iso-coordinates lines along the boundary. From figure 3.2 we have that boundaries ②, ③ and ④ will have the condition that states the location of the boundary in the ξ-direction; while the boundary condition in η-direction specify the distribution of the iso-coordinates lines along the boundary. The opposite happens for boundaries ① and ⑤: location of the boundary is defined in the η-direction and distribution of the iso-coordinates lines in the ξ-direction.

The boundary conditions in each side for each direction are enumarated as follows. The underlined direction is the direction that specify the location of the boundary.

① $\underline{\eta}$-direction: Position of iso-coordinates lines are fixed
ξ-direction: Position of iso-coordinates lines are fixed

② η-direction: Equally spaced iso-coordinates lines
$\underline{\xi}$-direction: Kinematic condition at liquid/gas interface

$$n \cdot \mathbf{v} = 0 \tag{3.2}$$

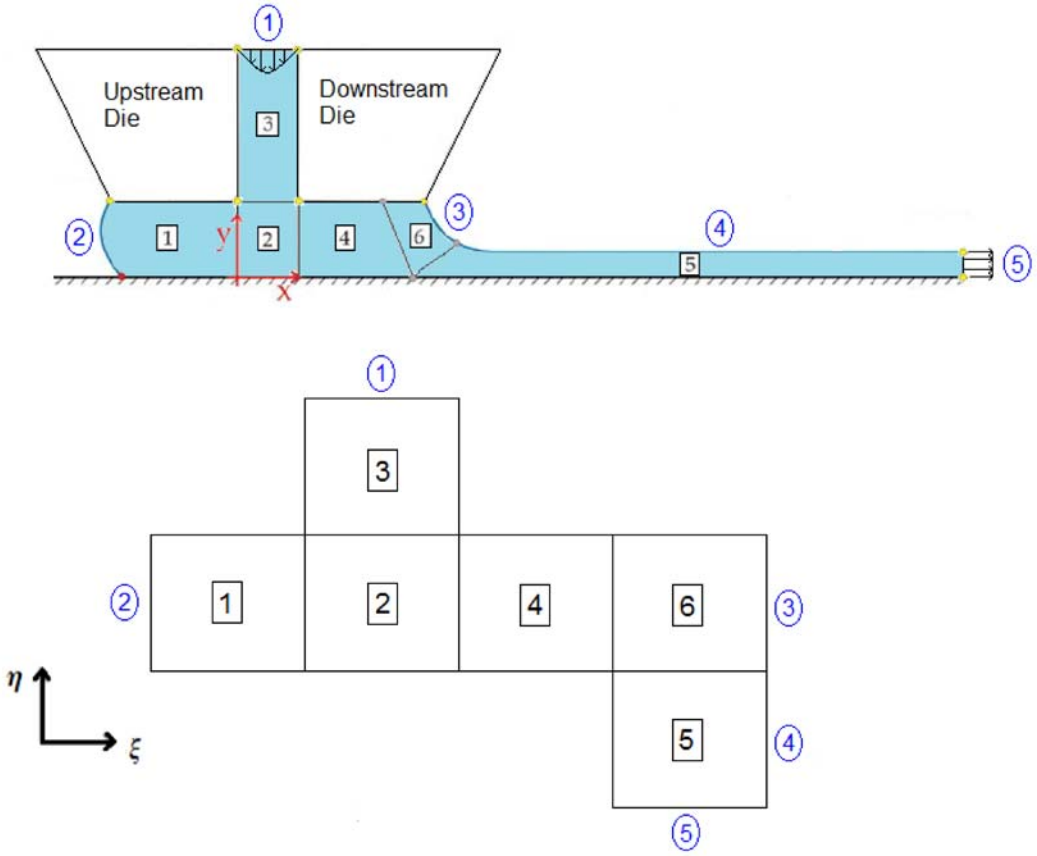

Figure 3.2: Geometry of the problem with boundaries enumarated in the physical and reference domains.

③ η-direction: Equally spaced iso-coordinates lines

$\underline{\xi}$-direction: Kinematic condition at liquid/gas interface

$$n \cdot \mathbf{v} = 0 \tag{3.3}$$

④ η-direction: Orthogonality

$$n \cdot \nabla\eta = 0 \tag{3.4}$$

$\underline{\xi}$-direction: Kinematic condition at liquid/gas interface

$$n \cdot \mathbf{v} = 0 \tag{3.5}$$

⑤ $\underline{\eta}$-direction: The geometry of the region side is defined and iso-coordinates lines slide over boundary.

ξ-direction: Orthogonality

$$n \cdot \nabla \xi = 0 \tag{3.6}$$

3.2 Finite Element Method - 2D element

The finite element method (FEM), a weighted residual method, is a general and systematic technique for obtaining approximate solutions of differential equations written in a weak form; i.e., it is a method of discretizing the weak form with the result that the underlying function spaces become finite - and thus manageable to representation via computer. The approximate solution is represented as a linear combination of approximation functions (basis functions) usually piecewise polynomials (e.g. linear, quadratic, or cubic) defined over the spatial domain of the problem.

The piecewise polynomials of the FEM are also called basis functions and are said to "span the space": any function in this finite-dimensional subspace is presumed to be representable by an appropriate linear combination of these basis functions. When the weightin functions used in the weak form are also represented by a linear combination of the same basis functions used to approximate the solution, the FEM that evolves is called the Galerkin Finite Element Method; which is the case of the present work. The basis functions are piecewise continuous and linearly independent, and their first derivative, while discontinuous (they typically suffer jumps at node points), are square integrable - Gresho and Sani (2000).

The particle transport equation has a term proportional to the divergence of the derivative of the deformation rate, i.e. proportional to the third derivarive of the velocity field. Even after applying the divergence theorem to reduce the order of the derivative of this term, one ends up with a second derivative of the velocity field. Since the basis functions used to represent the velocity field (piecewise polynomials) have discontinuous derivarive accross the element boundaries, it is necessary to represent the velocity gradient as an independent field, called G, with a continuos interpolation. This is the same approach used in the solution of viscoelastic flows by FEM (Szady et al. (1995)). The equation that describes the interpolate velocity gradient field G used in this work is:

$$G = \nabla \mathbf{v} - \frac{\nabla \cdot \mathbf{v}}{tr\,(\mathbf{I})}\mathbf{I} \tag{3.7}$$

The system of governing equations, eqs 2.2, 2.3, 2.4, 3.1 and 3.7, together with the appropriate boundary conditions was solved by Galerkin's method with quadrilateral finite elements. The weighted residual equations are obtained after multiplying each equation by weighting functions, integrat-

ing over the unknown flow domain, applying the divergence theorem to terms with divergences and mapping the integrals onto the known reference domain.

Each independent variable is approximated by a linear combination of a finite number of known basis functions, as shown in Table 3.1. The piecewise polynomial used as basis function for each field is also presented in Table 3.1.

Table 3.1: Piecewise polynomials used to expand the variables of the problem for a two dimensional element.

Variable	Expanded as	Basis function
u	$\sum u_j \phi_j$	Bi-quadratic
v	$\sum v_j \phi_j$	Bi-quadratic
x	$\sum x_j \phi_j$	Bi-quadratic
y	$\sum y_j \phi_j$	Bi-quadratic
c	$\sum c_j \phi_j$	Bi-quadratic
p	$\sum p_j \chi_j$	Linear discontinuous
G_{xy}	$\sum G_{xy_j} \psi_j$	Bi-linear
G_{xx}	$\sum G_{xx_j} \psi_j$	Bi-linear
G_{yy}	$\sum G_{yy_j} \psi_j$	Bi-linear
G_{yx}	$\sum G_{yx_j} \psi_j$	Bi-linear

Another useful and important property of the basis functions used is that they are Lagrange interpolating polynomials. This property gives the discrete system of equations a convenient property that the numerical value of the coefficient of the expansion is the value of the function on the given node.

Figure 3.3 shows the two-dimensional element used. The velocity field, mesh position and concentration field are evaluated in each of the 9 nodes. The pressure has three degrees of freedom and is evaluated in the center node, number 9. The continuous representation of the velocity gradient is evaluated in the corner nodes, i.e., nodes 1, 2, 3 and 4. Hence, each 2D element has 64 degrees of freedom.

3.3 Coupling Between 2D and 1D Elements

The mathematical formulation of the problem when surface tension dependency on particle concentration and particle transport from bulk to interface are considered involves one extra field: the surface particle concentration c_{int}. And one extra differential equation, the surface particle transport equation (eq.

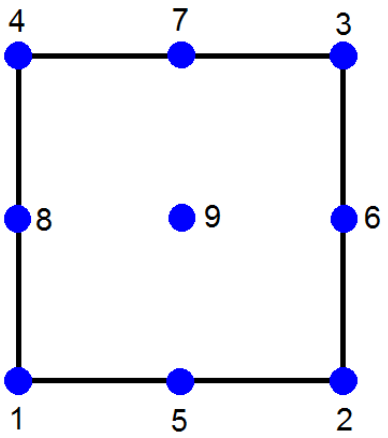

Figure 3.3: Two-dimensional element used for Galerkin FEM.

2.31) coupled with the net bulk-interface flux (eq. 2.29). The extra equation and field are only defined over the interface and therefore a 1-D finite element need to be used to discretize the problem. The new 1-D field is coupled with the 2-D fields, velocity and bulk concentration, hence the new 1-D finite elements need to be coupled with the 2-D finite elements used to represent the flow fields and bulk concentration.

Figure 3.4 shows how the 1D-element interacts with the 2D-element. As it is shown, the nodes of the one-dimensional element are physically the same as the nodes of the two-dimensional side where 1D-element lies; i.e., 1D-element overlaps 2D-element. Therefore, the unknowns (for example, velocity and position) have the same values for equivalent nodes in both elements.

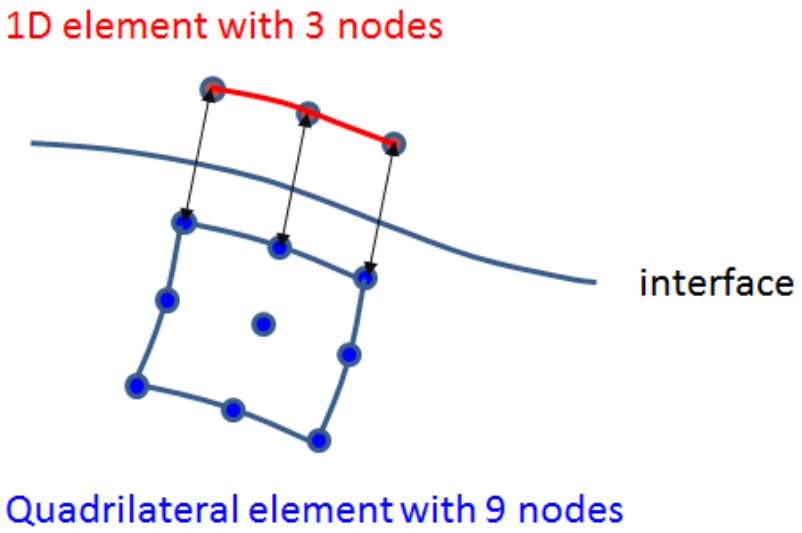

Figure 3.4: Scheme of the coupling between the two elements.

However, at the interface, surface particle concentration is also evaluated.

This field, interface concentration, is also expanded as a linear combination of quadratic basis function. The equation that describes the interface particle transport and the net flux from the bulk to the interface is also written in its weak form and incorporated to Galerkin Finite Element Method.

The degrees of freedom of the one-dimensional element are presented in Figure 3.5. Each node of an 1D-element has the same degrees of freedom of the equivalent 2D-element node, plus interface concentration. Finally, for a 1D-element there are 26 degrees of freedom. Table 3.2 presents the polynomials used as basis function for 1D element.

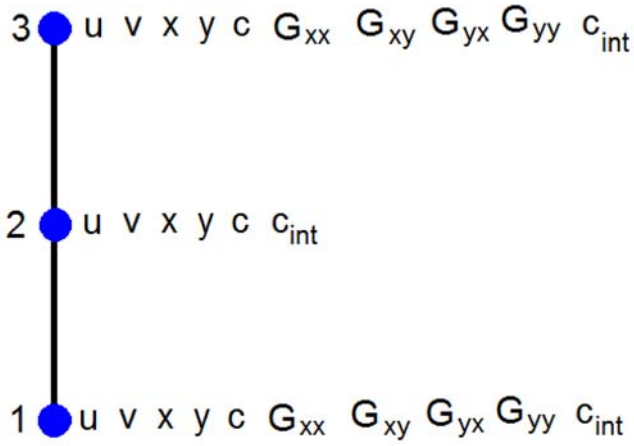

Figure 3.5: Degrees of freedom for the 1D-element.

Table 3.2: Piecewise polynomials used to expand the variables of the problem for one dimensional element.

Variable	Expanded as	Basis function
u	$\sum u_j \phi_j$	Bi-quadratic
v	$\sum v_j \phi_j$	Bi-quadratic
x	$\sum x_j \phi_j$	Bi-quadratic
y	$\sum y_j \phi_j$	Bi-quadratic
c	$\sum c_j \phi_j$	Bi-quadratic
G_{xy}	$\sum G_{xy_j} \psi_j$	Bi-linear
G_{xx}	$\sum G_{xx_j} \psi_j$	Bi-linear
G_{yy}	$\sum G_{yy_j} \psi_j$	Bi-linear
G_{yx}	$\sum G_{yx_j} \psi_j$	Bi-linear
c_{int}	$\sum c_{int_j} \phi_j$	Bi-quadratic

To couple 2-D flow with the 1-D surface particle tranport, the boundary integrals of the momentum conservation are evaluated over the 1-D finite elements, at which the local surface particle concentration degrees of freedom are available to evaluate the local surface tension.

3.4 Non-linear System of Algebraic Equations

Once all the variables are represented in terms of the basis functions, the system of partial differential equations reduces to a set of non-linear algebraic equations. The unknowns of this system are the coefficients of the finite element expansions: u_j, v_j, x_j, y_j, c_j, p_j, G_{xy_j}, G_{xx_j}, G_{yy_j} and G_{yx_j} (and c_{int_j}, for the case that considers bulk-interface particle transport).

This non-linear system was solved by Newton's method with numerical evaluation (central difference) of the Jacobian matrix entries.

Because the finite element basis functions used are different from zero over only a very small portion of the domain, the Jacobian matrix is sparse and was stored in compressed sparse format. In each Newtonian step, the linear system was solved by a frontal solver (direct method).

Different numbers of elements in each region of the mesh were tested. The first mesh tested is presented in figure 3.6. In order to obtain more accurate results, the number of elements in each region was increased and this second mesh is presented in figure 3.7. However, this second mesh increased the number of unknowns in a way that we could only obtain a converged solution for a small range of dimentionless parameters. Therefore, another configuration for the mesh is presented in figure 3.8, and is called mesh 3. Table 3.3 presents the total number of elements at each region of all cases studied.

Table 3.3: Total number of elements per region for all mesh tests.

Region	Mesh 1	Mesh 2	Mesh 3
1	80	100	80
2	64	80	40
3	80	96	28
4	96	150	80
5	150	270	300
6	80	150	150
Total	550	846	678

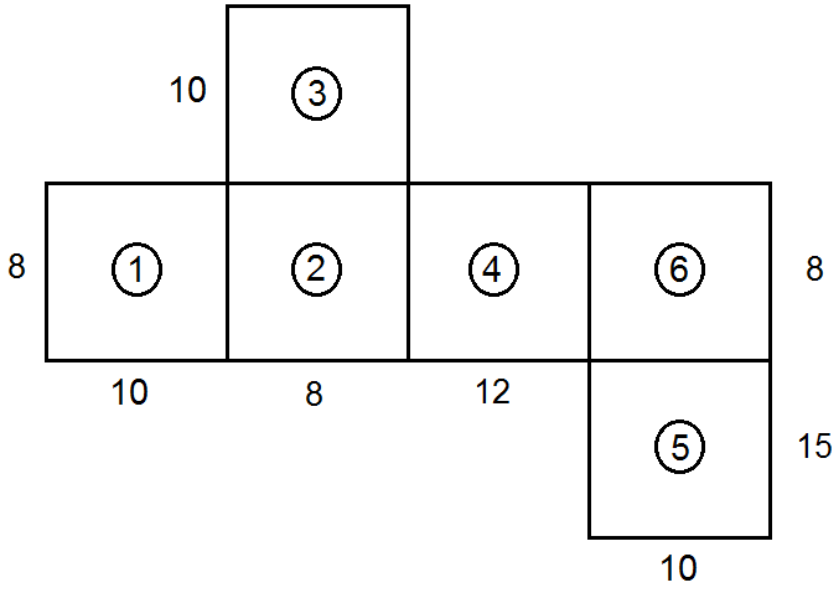

Figure 3.6: Numbers of elements in each direction for mesh test 1.

In order to validate the choice of the mesh, a problem was solved with both mesh 2 and 3. Figure 3.9 shows the results of the particle concentration distribution in the coated layer for those meshes. The case studied presents a final film thickness that is half of the gap, surface tension is considered constant, there is no sedimentation and the value of the migration mechanisms constants are: $K_c = 1.2$ and $K_\mu = 1.8$. As we can see, for those meshes the solution is mesh independent. Therefore, we use mesh 3 as it yields larger range of values of the parameters to be studied.

For the case that considered bulk-interface particle transport, two regions

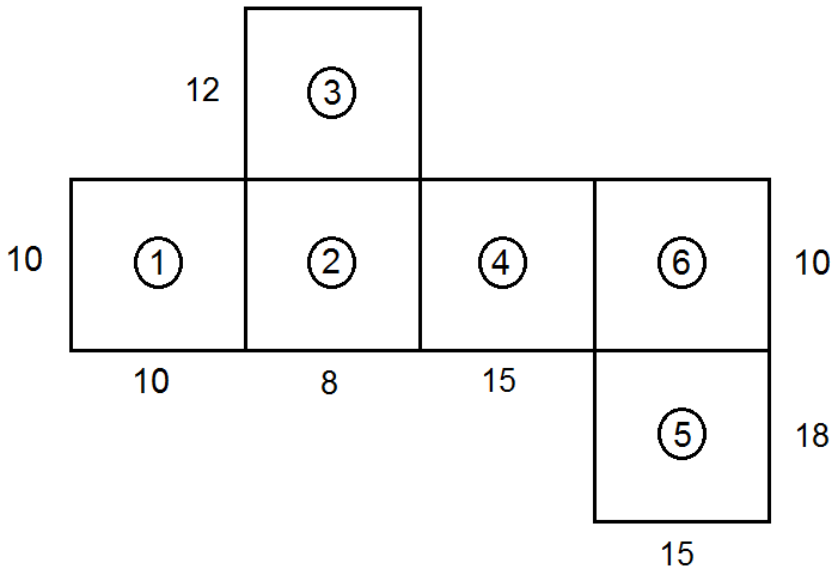

Figure 3.7: Numbers of elements in each direction for mesh test 2.

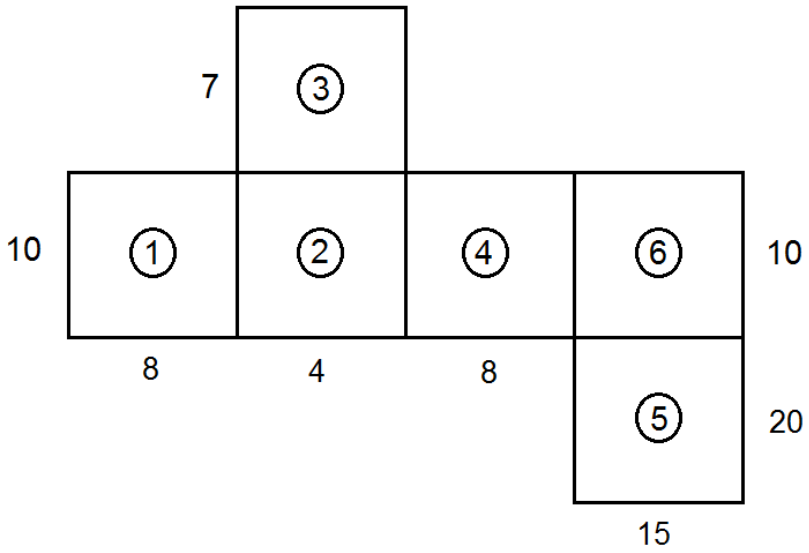

Figure 3.8: Numbers of elements in each direction for mesh tests 3, used in the present work.

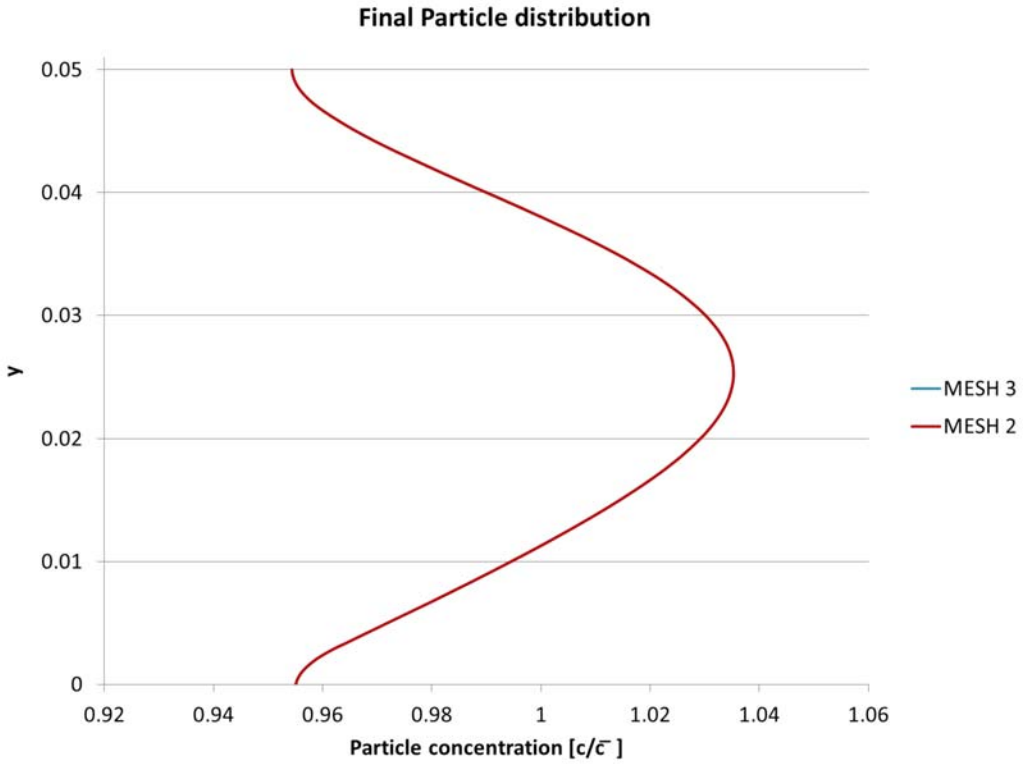

Figure 3.9: Final particle distribution using Mesh 2 and Mesh 3.

of 1D elements are added to the mesh as presented in figure 3.10. The number of degrees of freedom was 19323 for the purely 2D analysis, and 19384 for the coupled 2D/1D cases.

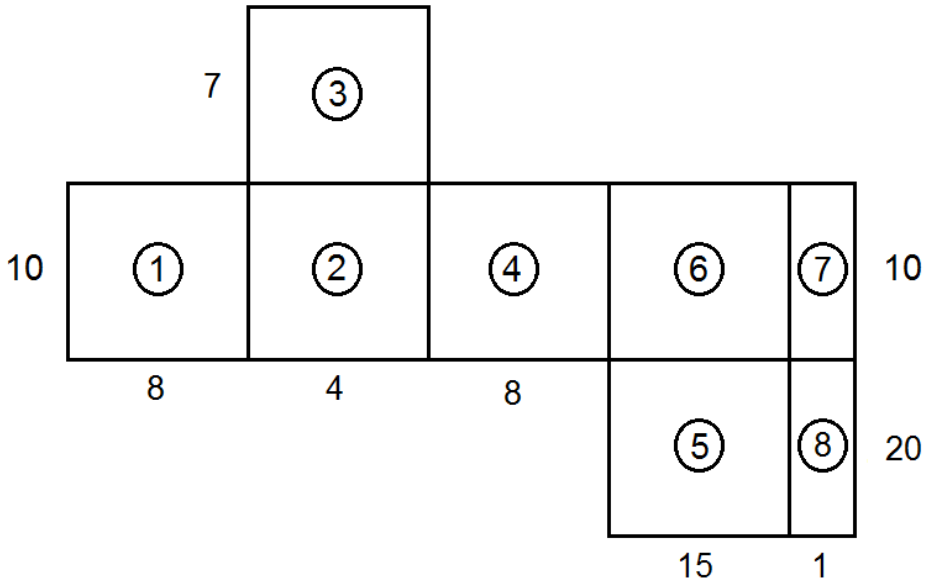

Figure 3.10: Numbers of elements in each direction for mesh used in the present work when surface particle concentration is also evaluated.

4
Qualitative Slot Coating Flow Analysis

Before presenting the results, we will analyse the basics of slot coating flow characteristics because different diffusion mechanisms acting in different areas of the flow will affect the final particle distribution. Therefore, it is important to understand flow configuration on each region and how does it influence particle migration. For instance, the first two migration mechanisms - due to shear rate gradient and viscosity gradient - explained in Chapter 2 are a function of the flow. Hence, understanding the flow in different areas of the coating process will help to comprehend the overall particle migration and, consequently, the final particle distribution.

Slot coating flow can be sub-divised in five different regions: fed slot region, upstream region, transition region, downstream region and film formation region. These different areas are shown in Figure 4.1.

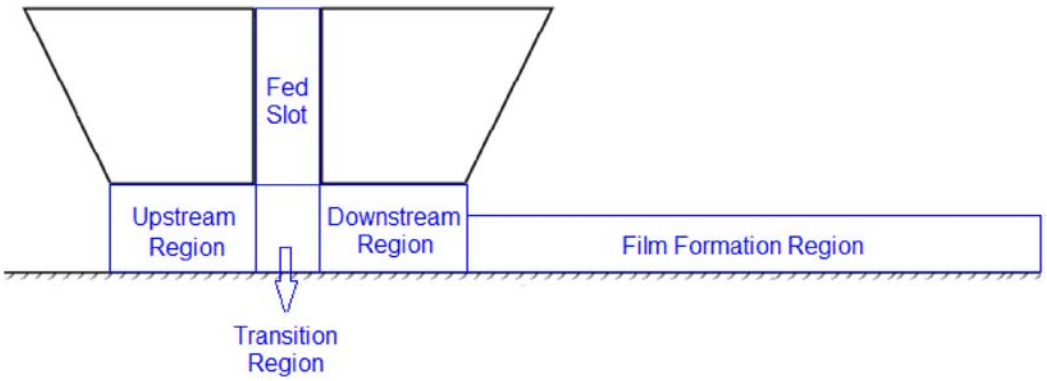

Figure 4.1: Sub-division areas of the coating flow.

The transition flow region is just the area under the fed slot, and between the downstream and upstream regions. What happens in this region does not strongly affect the final particle distribution, hence it will not be analysed in further details in this Chapter. The equivalent will happen to the upstream region; as the flow under the upstream die also does not play a significant role at the particle distribution on the coated layer.

As mentioned earlier in Chapter 2, the first migration mechanism is related to the shear rate profile. If the shear rate is not constant then particles will migrate from higher shear rate areas to lower shear rate areas. If particle

distribution is non-uniform, then there will be a second migration mechanism where particles migrate from higher viscosity areas to lower viscosity areas. Depending on the region of the coating flow, one of these mechanisms will act more than the other. A qualitative analysis is shown in the following sections. A quantitative analysis is presented in Chapter 5.

4.1 Fed Slot Region

The flow at the fed slot region may be seen as a pressure driven between two parallel plates flow. As a consequence, the velocity profile will be parabolic and the shear rate profile will present the lowest values closest to the center of the channel. Therefore, particle will migrate towards the center of the fed slot due to the shear rate gradient mechanism.

The viscosity gradient mechanism may change the particle profile in order to make it more uniform. However, if the viscosity gradient mechanism is not strong enough then there will still be a higher particle concentration at the center of the fed slot. The suspension flow in a tube has been experimentally studied and it shows that indeed the particle concentration is higher at the center of the tube (Phillips et al. (1992)).

4.2 Downstream Region

The flow under the downstream die is a combination of two different flows:

1. Couette flow: due to the drag of the web.
2. Poiseuille flow: due to pressure difference.

Assuming that the web speed is constant, then depending on the imposed flow rate (film thickness) there will be a different Poiseuille flow contribution. The dependency of the final particle distribution on the film thickness has been extensively studied in Silva and Carvalho (2013). A summary of particle concentration field at different thickness are presented in Figure 4.2 (**P**HF stands for the particle concentration).

As it is shown in Figure 4.2, depending on the imposed film thickness there will be a different Poiseuille contribution. The thinner the film thickness is, the greater is the adverse Poiseuille contribution. The blue areas at the velocity profiles highlight the zero shear rate area, where particles will tend to migrate to. On the right hand side of the figure it can be seen that indeed there is a higher particle concentration in the highlighted blue areas.

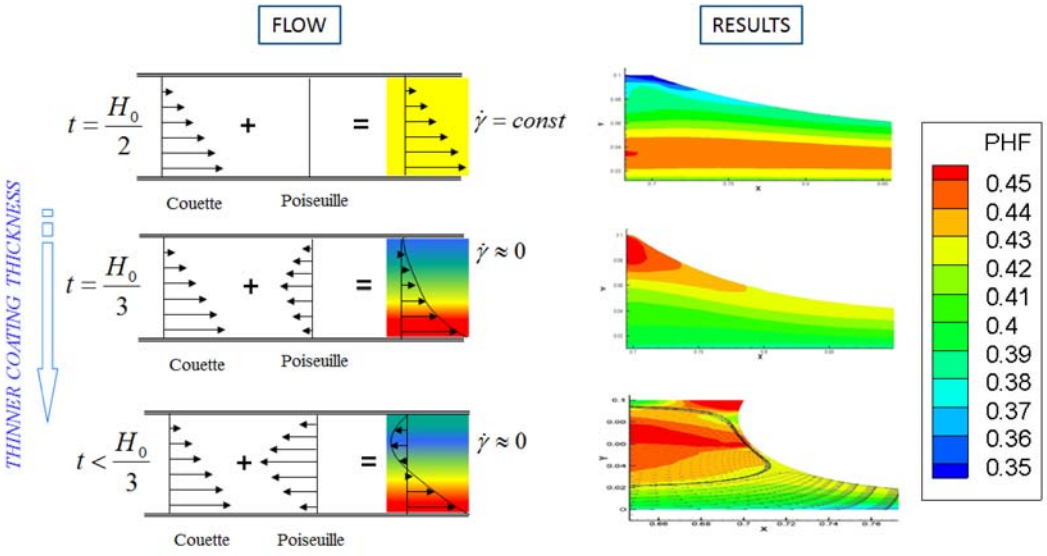

Figure 4.2: The final particle distribution as a function of the film thickness.

In the first case where the film thickness is one half of the gap something interesting takes place. Even though the velocity profile is linear and, therefore, there is no shear rate gradient, the particles are more concentrated in the middle of the film. This may be explained by the fact that at the fed slot the particle concentration is higher at the center of the film and, as there is no particle migration due to shear rate gradient at the downstream flow, the particle distribution at the fed slot will be convected through the film given a higher concentration at the center of the coated film. For the other cases it can be seen that particle concentration is higher at the top of the film.

That study, however, simulated coating process for fixed values of the migration mechanisms constants. In Chapter 5 we study final particle distribution for different values of those constants and we see that the absolute value of those constants may affect the final particle distribution. The reasons why this happens may be better understood by the analyse of the last region.

4.3 Film Formation Region

At the coated film, the velocity profile is constant and equal to web speed. Accordingly, the shear rate is zero and there will be only particle migration due to viscosity gradient. Furthermore, the input of particle profile at the film formation region is the output of the particle profile at the downstream region. Therefore, the final particle distribution will be a function of the particle distribution under the downstream die and the diffusion mechanism due to viscosity gradient. The effect of the relative contributions of each mechanism at the final particle distribution will be presented in Chapter 5. However, we may

make some primary conclusions from a qualitative analysis. These conclusions are presented below:

1. The particle profile at the end of the downstream region must be non-uniform in order to induce diffusion migration due to viscosity gradient at the final region.
2. If the particle profile is non-uniform, then the viscosity gradient diffusion mechanism will act in order to make the particle profile more uniform; taking particles from higher viscosity area (or higher particle concentration area) to lower viscosity areas (or lower particle concentration area).
3. Finally, if the migration mechanism due to viscosity gradient is strong enough it will change the particle profile and make it more uniform. Otherwise, the final particle distribution will be mostly a function of the particle distribution at the downstream region.

5
Results

This Chapter presents the results of the model developed and it is subdivised in different sections. In the first section, we study the flow and the final particle concentration distribution as a function of the dimentionless parameters defined in Chapter 2 for a film thickness that is half of the gap. In section 5.2 a similar study is made but for a final film thickness that is one forth of the gap. In the next section, section 5.3, the surface tension gradient effects on the flow and particle distribution is study. First, we consider that particle migration form the bulk to the interface is instantaneous and, as a consequence, particle concentration along the interface is the same as bulk concentration. Then, in section 5.4, particle transport from the bulk to the surface is considered and particle concentration along the interface is no longer equal to bulk concentration.

As presented in Figure 4.2, we expect particle concentration to be higher in the middle of the film for the case where the film thickness is half of the gap. Besides, for the case where the film thickness is one forth of the gap, the higher particle concentration is expected to be at the top of the film.

For all cases presented below $Ca = 0.05$.

5.1
Results: $h = 2$

In this section, particle distribution is studied as a function of some dimentionless parameters. The goal of this section is to understand the effect of Pe, k and S on the particle profile for a film thickness that is half of the gap. First, Pe effect is studied. Then, Pe assumes a constant value and k is studied. Finally, with a fixed value for Pe and k, sedimentation effect is studied.

5.1.1
Effect of Pe

As presented in Chapter 2, Peclet number is the ratio between convective and diffusive particle transports. Figure 5.1 shows particle concentration along the film thickness for different values of Pe. The x-axis of figure 5.1 shows particle

concentration normalized by average particle concentration (which in this case is 0.4). The y-axis is the height of the film thickness, $t = 0.05mm$.

As Pe is a function of K_c, K_c assumes different values in order to vary the value of Pe. However, to keep the other dimentionless parameters constant, such as k ratio, we also change K_μ so k remains constant and equal to 0.4. The S parameter is not a function of K_c, neither K_μ; and is set at $S = 0.0$ for the results shown in this section.

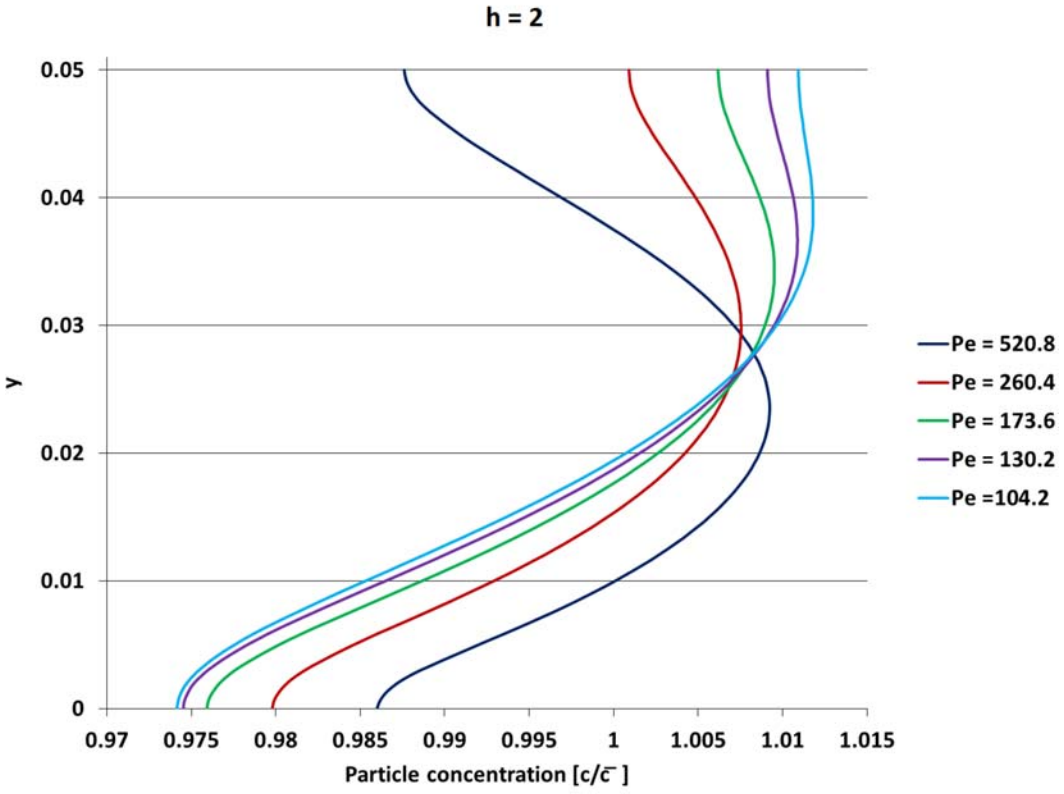

Figure 5.1: Final particle distribution at the coated layer for different values of Pe where $h = 2$ ($k = 0.4$, $S = 0$ and $Ca = 0.05$).

As discussed in Chapter 4, for this configuration where the film thickness is half of the gap, the expected outcome is to have higher particle concentration in the middle of the coated layer as there is no particle transport due to shear rate in the downstream region and particle distribution at the fed slot (higher concentration in the middle of the flow) is convected through the film. However, figure 5.1 shows that this might be not always right. Different Pe numbers yields different particle concentration profiles.

Figure 5.1 shows that at $Pe = 520.8$ particle concentration is indeed higher in the middle of the film; which means that convective transport is stronger enough than diffusive transport so particle distribution at the fed slot is convected through the film. On the other hand, as Pe number falls, diffusive

transport increases. Figure 5.1 also shows that for $Pe \leq 260.4$ particles, instead of being more concentrated in the middle of the film, migrate towards the top of the film. To understand why particle profile changes we must take a look at the velocities profiles in different regions of the flow. Figure 5.2 sketches the velocity profiles at downtream and film formation regions for this configuration. Because the thickness is half of the gap, the flow under the downstream die is a pure Couette flow.

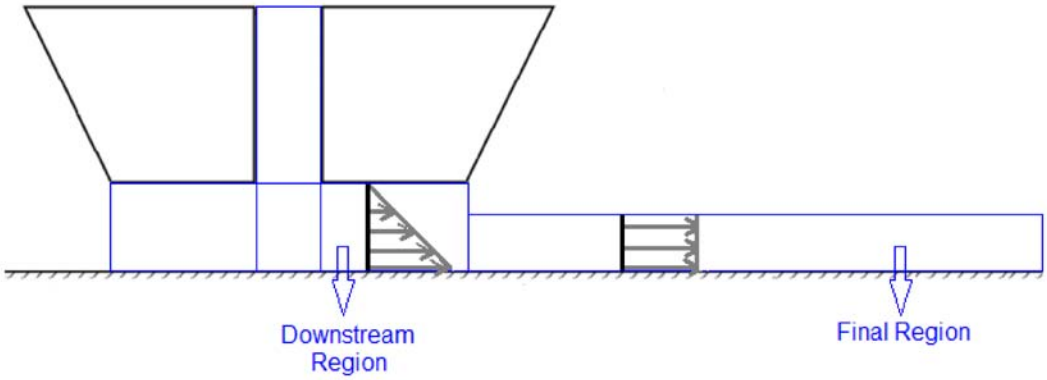

Figure 5.2: Velocity profiles when $h = 2$.

In both regions the velocity profile is linear and shear rate is constant. First, looking at the downstream region: the input particle profile for this region is the output of the fedslot; which means higher particle concentration in the center. As diffusion particle transport increases, particle profile becomes more uniform along the downstream region because there is no particle migration due to shear rate gradient, only migration due to viscosity gradient; this last mecanism acts in the opposite direction of the concentration gradient, making particle distribution more uniform along the film. Yet, at the end of the downstream region, velocity profile changes as the flow evolves from a flow between two walls to a flow with a liquid-air interface. The velocity profile under the downstream die is linear and in the position $y = H_0$, no-slip condition is applied and velocity is zero (Figure 5.2). However, when the flow reaches the downstream free surface, boundary condition states that shear rate along the surface is zero. As a consequence, while the velocity profile is changing to become linear again in the film formation region, there is particle migration towards the top of the film - zero shear rate area. As flow develops, the shear rate approaches zero, hence there is no particle migration due to shear rate gradient. Therefore, for lower Pe particles migrate towards the top of the film as figure 5.1 shows. This result show how complex kinematics in the film formation region can affect the particle distribution in the coated layer.

Figure 5.3 shows the concentration field at $Pe = 260$, in which indeed

particle concentration gradient is smoothed in the downstream region (legend 'PHF' stands for concentration field). In this figure we can see that at the fed slot region particles concentrate in the middle of the flow channel. At the transition region, particle concentration starts to be smoothed by particle migration mecanisms. For the following regions, figure 5.3 is not very clear but some analysis are made. Along the downstream region, particle concentration becomes even more uniform. In the film formation region, particles are transported in the direction of the free surface, or the zero shear rate area. As a consequence, at the final region particle concentration ends up higher at the top of the film.

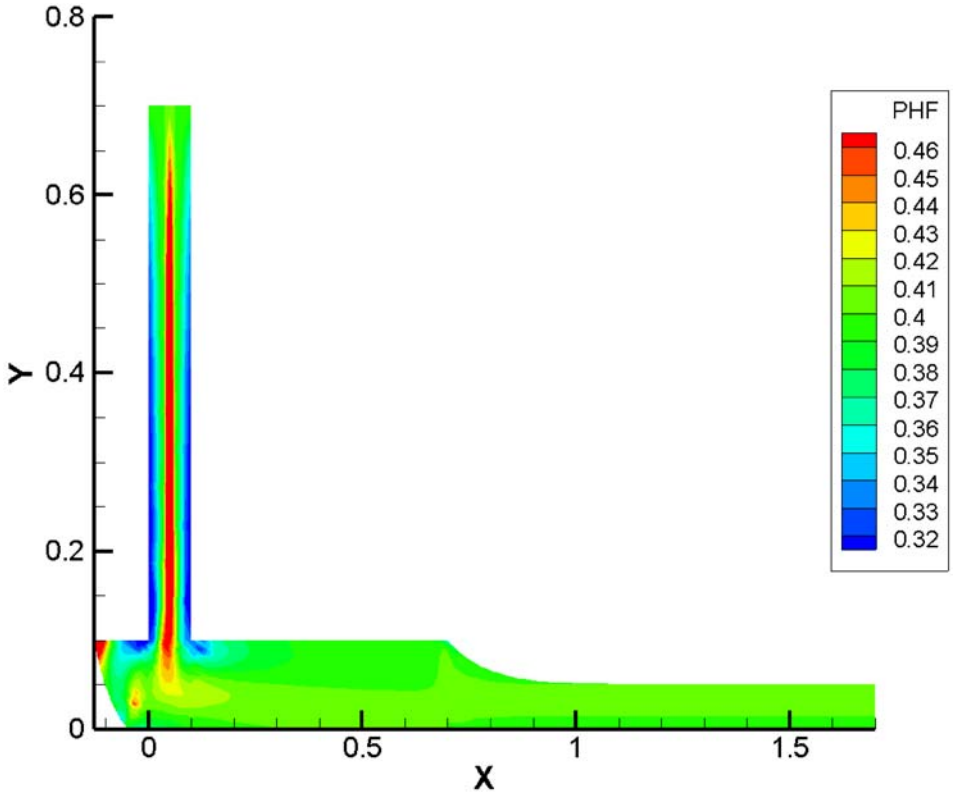

Figure 5.3: Concentration field for $Pe = 260$ ($k = 0.4$, $S = 0$, $Ca = 0.05$ and $h = 2$).

This smoothing effect on the downstream region is better showed in figure 5.4. This figure presents the concentration field at the downstream region for the case $Pe = 104$ at which convective transport is even weaker, when compared to diffusive transport. Not only the coating process was zoomed in, but also the concentration scale on the right hand side of the figure has been enhanced. This figure shows particle concentration gradient in more details. Even though the range for the concentration field is very small, there are areas with very uniform particle concentration. For instance, in the area closer to $x = 0.5$ concentration distribution becomes completely uniform ($c \approx 0.407$).

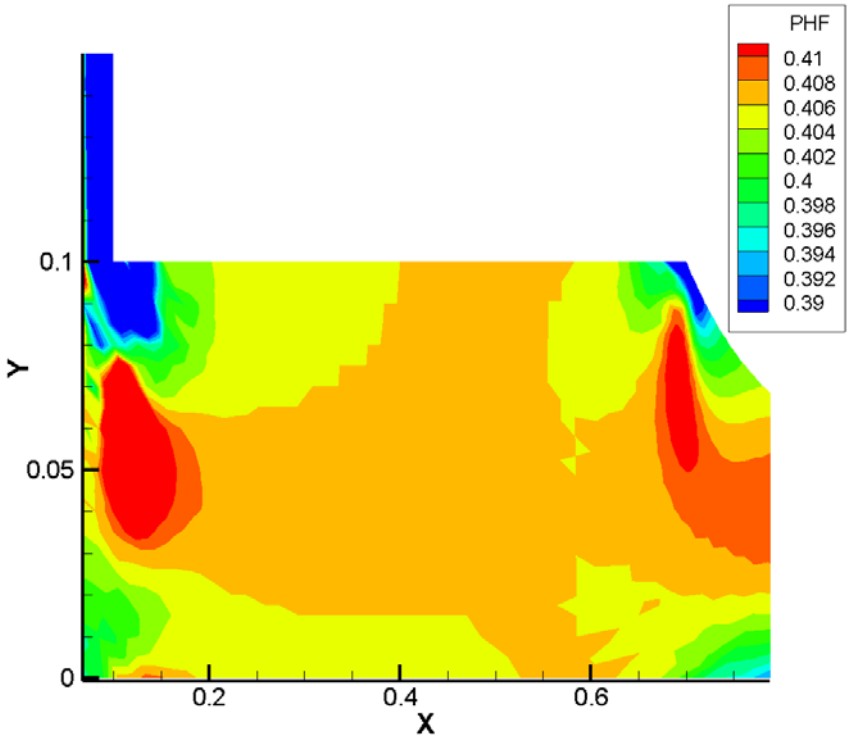

Figure 5.4: Concentration field for $Pe = 104$ at the downstream region ($k = 0.4$, $S = 0$, $Ca = 0.05$ and $h = 2$).

Another important conclusion from figure 5.1 is that particle concentration at the top of the film does not increase linearly with Pe number. In fact, particle concentration difference between cases $Pe = 520$ and $Pe = 260$ is greater than the difference between cases $Pe = 260$ and $Pe = 130$ at $y = t$. This behavior happens because as Pe decreases, diffusion transport increases. As said before, at the film formation region shear rate is zero and there will be no particle migration due to shear rate gradient. However, there will be particle migration due to viscosity gradient which will pump particle away from higher concentration areas, in the direction of lower concentration areas. In other words, as Pe decreases, K_μ increases, reducing particle gradient. As a consequence, particle profile does not change linearly with Pe due to the intensity of viscosity gradient migration mechanism.

Before proceeding in the parametric analysis, Peclet number is fixed at 104.2. This value was choosen because it gives the most non-uniform profile. For this configuration we now analyse effect of the ratio between the diffusion coefficients, k.

5.1.2
Effect of $k = K_c/K_\mu$

As defined in Chapter 2, k is the ratio between the diffusion coefficients constants of shear rate gradient over viscosity gradient mecanisms. Therefore, lower values of k represents greater contribution of viscosity gradient migration mecanism. Likely, higher values of k represents greater contribution of shear rate gradient migration mecanism.

As mentioned before in the results presented in this section, Peclet number is set at 104.2. To study the effect of k, we have changed the value of K_μ. The predicted particle concentration profile along the coated film at different values of k are shown in figure 5.5. The x-axis of figure 5.5 shows particle concentration normalized by average particle concentration (which in this case is 0.4), as in figure 5.1 and all others future figures that present particle concentration profile along the film thickness.

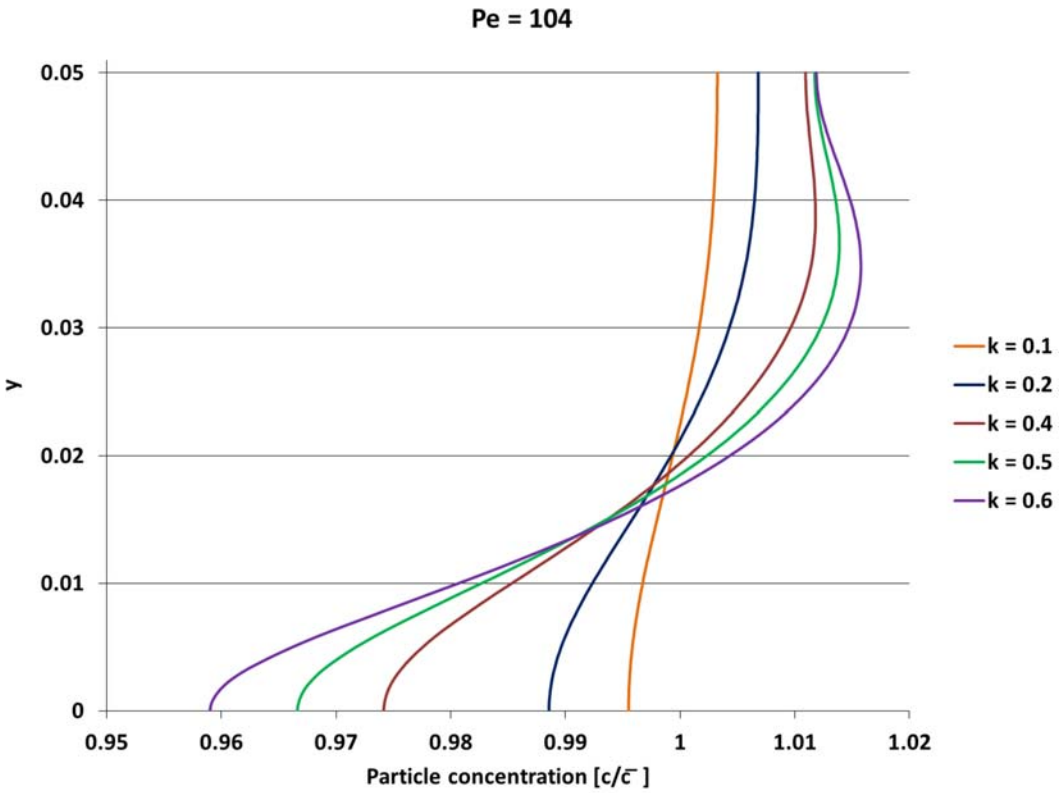

Figure 5.5: Final particle distribution at the coated layer for different values of k where $Pe = 104$ ($S = 0$, $Ca = 0.05$ and $h = 2$).

The reference value for k is $k = 0.4$; which was the value of k used in the previous subsection. As k increases ($k = 0.4$ to $k = 0.6$), the relative contribution of migration mecanism due to shear rate also increases. Thus, the phenomena described in the previous subsection, in which particle

concentration is higher at the top of the film, become more intense resulting on a more extreme particle profile; figure 5.5 presents this behavior.

In addition, when k ratio decreases ($k = 0.4$ to $k = 0.1$), the relative contribution of migration mecanism due to viscosity gradient increases. This migration mecanism tend to make particle distribution more uniform by reducing particle concentration gradient. Also, figure 5.5 shows that when $k = 0.1$ the particle distribution is extremely uniform. Finally, we may conclude that low values of k result in more uniform particle distribution, and the opposite happens to high values of k.

The effect of particle sedimentation, presented in the following section is analysed for two different values of k, the two most extreme values presented in figure 5.5 ($k = 0.1$ and $k = 0.6$). The results for S effect are shown in the next subsection.

5.1.3 Effect of Particle Sedimentation S

The first analysis is at $k = 0.1$. Figure 5.6 shows results for final particle distribution along the coated layer for different values of density difference between particles and liquid. We can note that the particle distribution at $S = 0$ is almost uniform. As density difference increases particle concentration at the top of the film decreases, and particle concentration at the bottom of the film increases; i.e., particle sedimentation becomes more important.

The sedimentation effect on the particle distribution was also present in the second case, at $k = 0.6$. The results for this case are presented in Figure 5.7. As it was explained in the previous subsection, due to the relative contribution of different migration mecanisms, the resulting concentration profile with no sedimentation ($S = 0.0$) shows higher particle concentration at the top of the film and lower particle concentration at the bottom of the film. As it would be expected, the additional migration mecanism due to sedimentation displaces particle from the top of the film to the bottom. As S rises and sedimentation becomes stronger, more particles are located at the bottom of the film, as expected.

Although the effect of sedimentation was observed in both cases at the top and bottom of the concentration profiles, the particle concentration in the middle of the film, i.e. $0.1 \leq y \leq 0.4$, did not change much. To understand which mecanisms are mainly acting in those cases and affecting the particle distribution we can take a look to the values of S parameter in each case. Those values are shown in table 5.2 along with the density difference between particles and liquid for each case. Table 5.1 shows the dimensional parameters

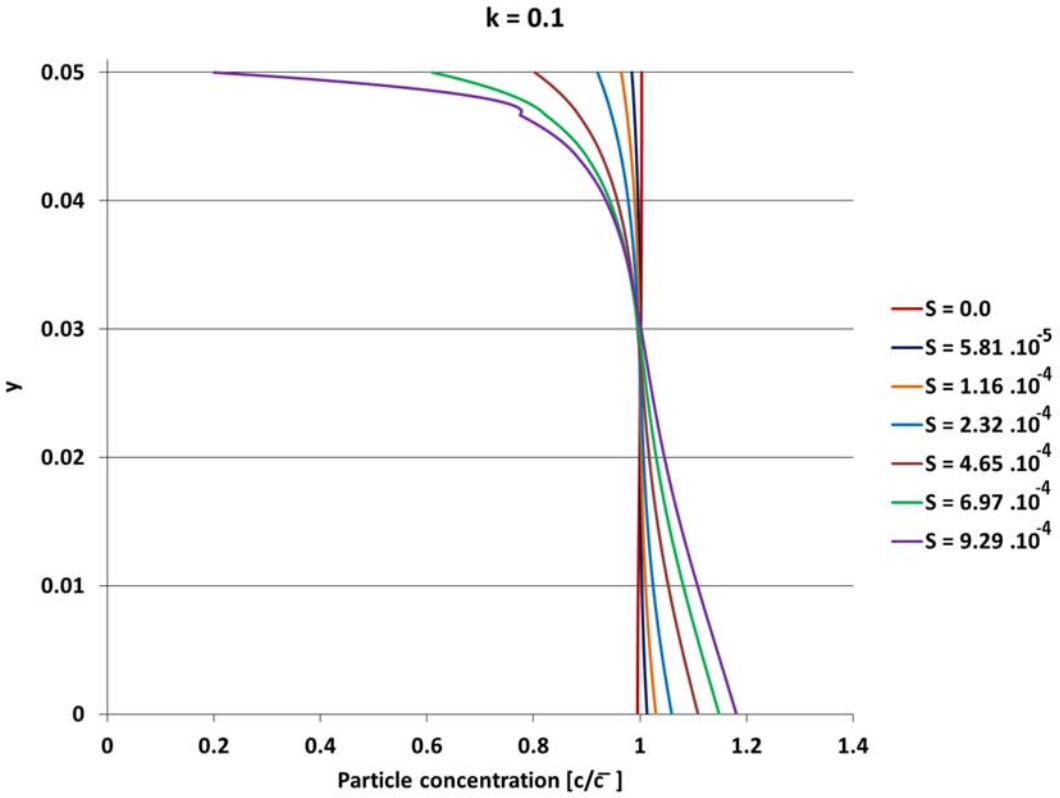

Figure 5.6: Final particle distribution at the coated layer for different density difference between particle and liquid, where $k = 0.1$ ($Pe = 104.2$, $Ca = 0.05$ and $h = 2$).

of the flow that are used to evaluate S values presented in table 5.2.

Table 5.1: Characterists of the flow, liquid and particles for all simulations.

Parameter	Value
a	0.004 mm
g	9.8 m/s^2
V	100 mm/s
μ_l	0.03 mm^2/s

The S parameter for all cases is very small. Therefore, convective tranport is stronger than sedimentation. In other words, sedimentation is not the main transport mecanism to affect all particle profile; it only changes certain areas of the film for the density differences tested. The range of density difference tested is appropriate for the coating process; it covers density difference between liquid (usually water) and different particles, such as polyester to silver particles.

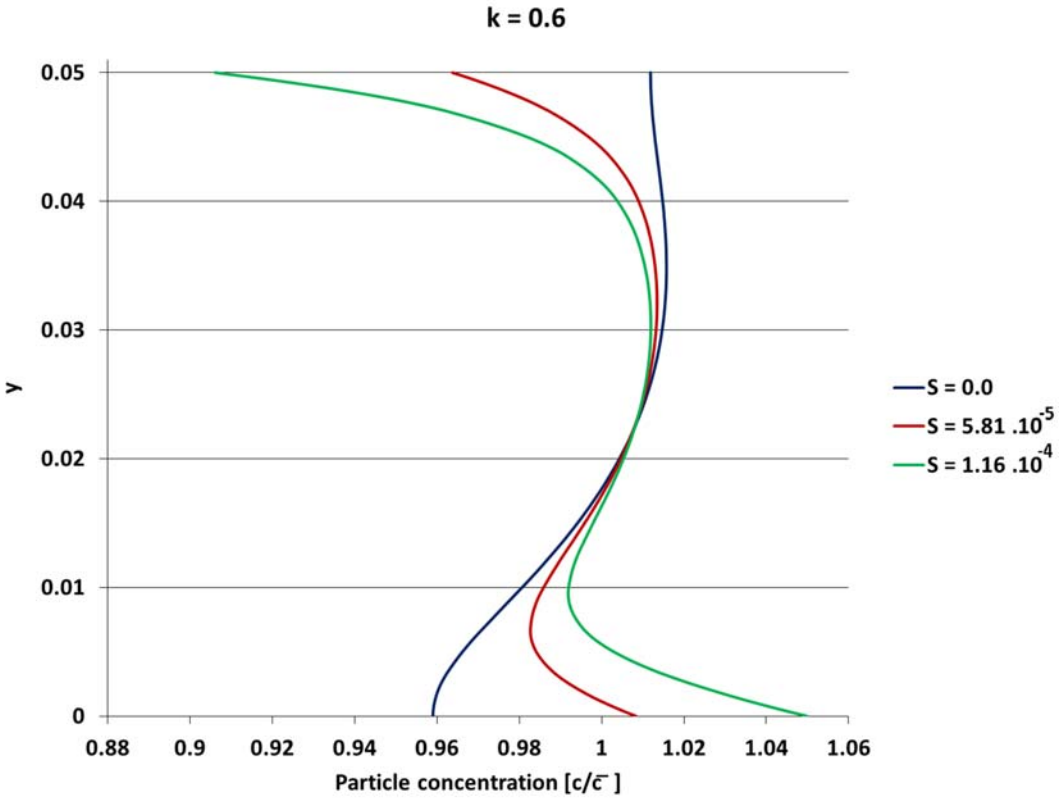

Figure 5.7: Final particle distribution at the coated layer for different density difference between particle and liquid, where $k = 0.6$ ($Pe = 104.2$, $Ca = 0.05$ and $h = 2$).

Table 5.2: Values of S parameter for the cases of Figures 5.6 and 5.7.

	$\Delta\rho$ $[g/mm^3]$	S
$k = 0.1$	0.0	0.0
	5.10^{-3}	$5.81 \cdot 10^{-5}$
	1.10^{-2}	$1.16 \cdot 10^{-4}$
	2.10^{-2}	$2.32 \cdot 10^{-4}$
	4.10^{-2}	$4.65 \cdot 10^{-4}$
	6.10^{-2}	$6.97 \cdot 10^{-4}$
	8.10^{-2}	$9.29 \cdot 10^{-4}$
$k = 0.6$	0	0.0
	5.10^{-3}	$5.81 \cdot 10^{-5}$
	$1..10^{-2}$	$1.16 \cdot 10^{-4}$

5.2 Results: $h = 4$

In this section we analyse the results for a film thickness that is one forth of the gap. Three dimentionless parameters are studied: Pe, k and S. The

present configuration usually yields high particle concentration gradient along the interface, as figure 4.2 shows. As explained before, at $h = 4$, the velocity profile under the downstream die lip yields a region of close to zero shear rate near the die wall, and particles are transported towards the top of the channel, and hence to the top of the film. Consequently, we expect that capillary effects will be more important when $h = 4$ than $h = 2$. As a consequence, next section - which evaluates capillary effect - uses the configuration where film thickness is one forth of the gap.

5.2.1 Effect of Pe

Figure 5.8 shows concentration profiles as a function of Peclet number for a film thickness that is one forth of the gap. Predictions are at $k = 0.4$ and $S = 0.0$. This figure shows that particle concentration distribution is very sensitive to Pe. Moreover, the dependency is not a monotonic function. Still, for all cases particle concentration was higher at the top than the bottom of the film, as it described Silva and Carvalho (2013).

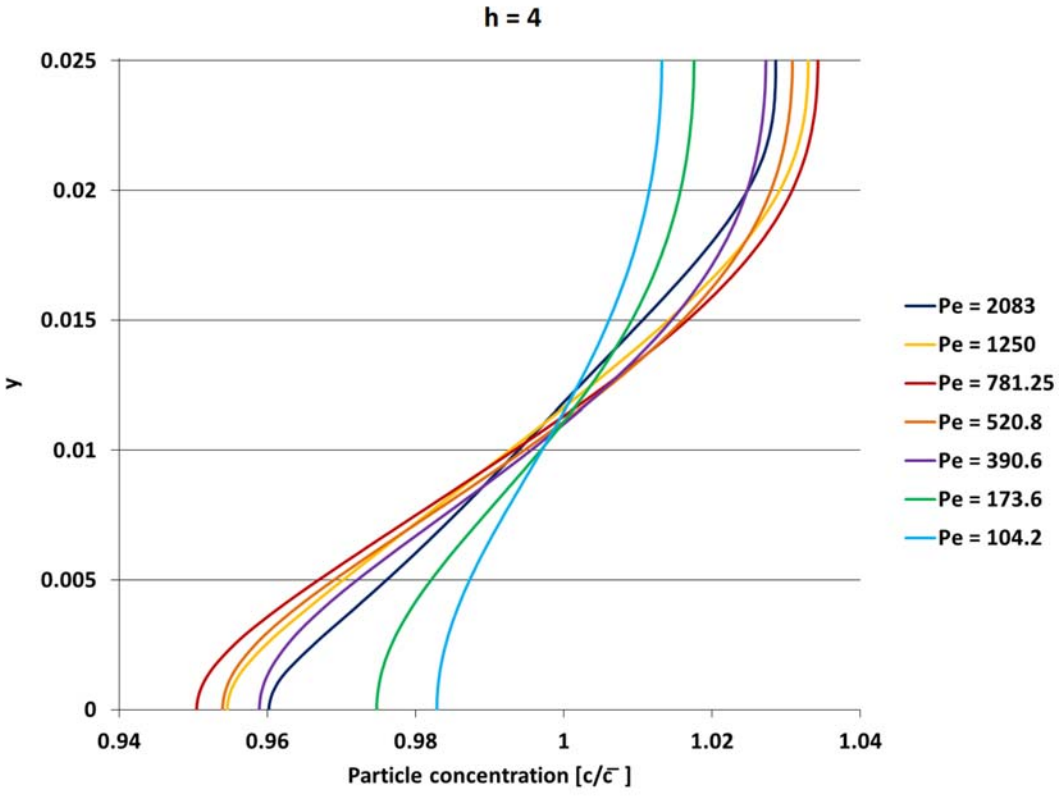

Figure 5.8: Final particle distribution at the coated layer for different values of Pe where $h = 4$ ($k = 0.4$, $S = 0$ and $Ca = 0.05$).

At high values of Pe, e.g. $2083 \geq Pe \geq 781.25$, as Pe decreases, particle

concentration at the top of the film increases, while at the bottom it decreases. Figure 4.2 shows the velocity profile at the downstream region when the film thickness is $t < H_0/3$ and it highlights the zero shear rate area near the die lip wall. Particles will migrate toward the zero shear rate area due to shear rate gradient migration mecanism, being more concentrated at the top of the film. As Pe decreases diffusion transport increases. As a consequence, as Pe decreases particles will be more displaced due to shear rate gradient mecanism; increasing particle concentration at the top of the film and decreasing at the bottom. However, for values below 781.25 concentration at the top of the film starts to decrease and the opposite happens to the bottom of the film.

As it was described in section 4.3, in the film formation region there is no particle migration due to shear rate gradient, only due to viscosity gradient. In addition, particle migration due to viscosity gradient makes particle distribution more uniform as it acts in the opposite direction of particle concentration gradient. As a conclusion, for cases where $Pe < 781.25$, viscosity gradient migration mecanism is strong enough to change particle distribution and makes it more uniform.

To sum it up, as Pe decreases particle concentration increases at the top and decreases at the bottom of the film due to shear rate gradient migration mechanism, up to a point at which viscosity gradient migation mecanism strongly affects particle profile inducing the inverse behavior and making particle profile more uniform. Figures 5.9(a), 5.9(b) and 5.9(c) corroborate this explanation.

At the downstream region, shear rate is not constant for this value of film thickness such that particles migrate towards the zero shear rate region near the die lip wall. As Pe decreases, diffusion tranport becomes stronger, and there will be more particles migrating to the zero shear rate area. As figures 5.9(a), 5.9(b) and 5.9(c) shows, as Pe decreases particle concentration under the downstream die increases - red area at the top of the downstream region grows. However, to understand the final particle distribution it is necessary to analyse the flow at the film formation region.

Figures 5.10(a), 5.10(b) and 5.10(c) present particle concentration field for each case in the film region. As Pe falls from $Pe = 2083$, 5.10(a), to $Pe = 781.25$, 5.10(b), the shear rate gradient mecanism becomes stronger leading to a higher concentration of particles on the top of the coated layer. At even lower Pe, 5.10(c), the viscosity gradient mecanism is strong enough to promote particle migration from the high concentration (high viscosity) to low concentration (low viscosity) region making the concentration distribution more uniform. Besides, high Pe means low K_μ. Then, at figures 5.10(a) and

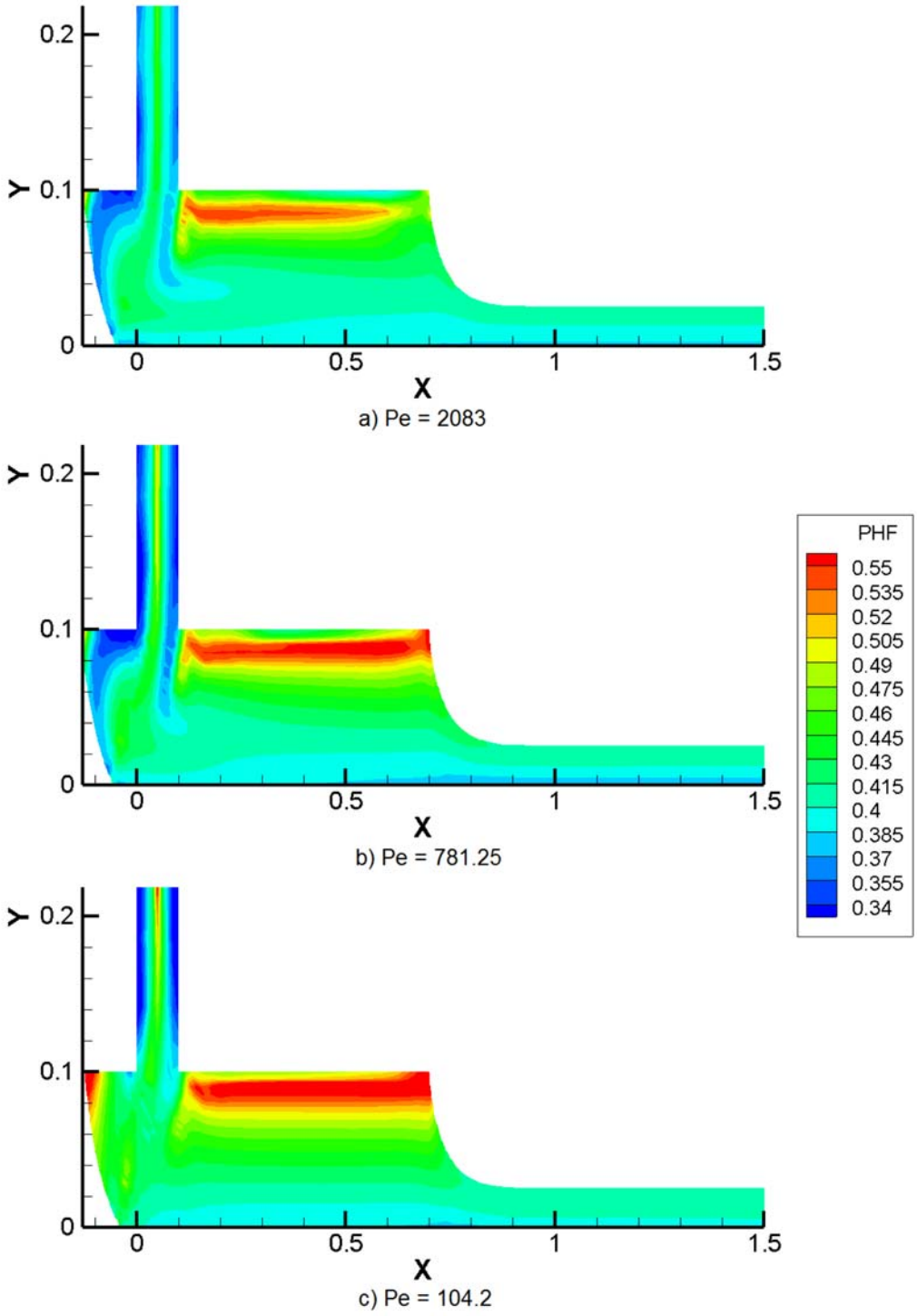

Figure 5.9: Concentration field for different values of Pe and $h = 4$ ($k = 0.4$, $S = 0$ and $Ca = 0.05$).

5.10(b) particle distribution does not change much along the final region. However, for the $Pe = 104$ case, there is a significant difference on the particle profile between the entrance and the end of the film formation region.

The case $Pe = 781$ is used to study the effect of the diffusion constants ratio k at $h = 4$ because this case presents the most non-uniform particle

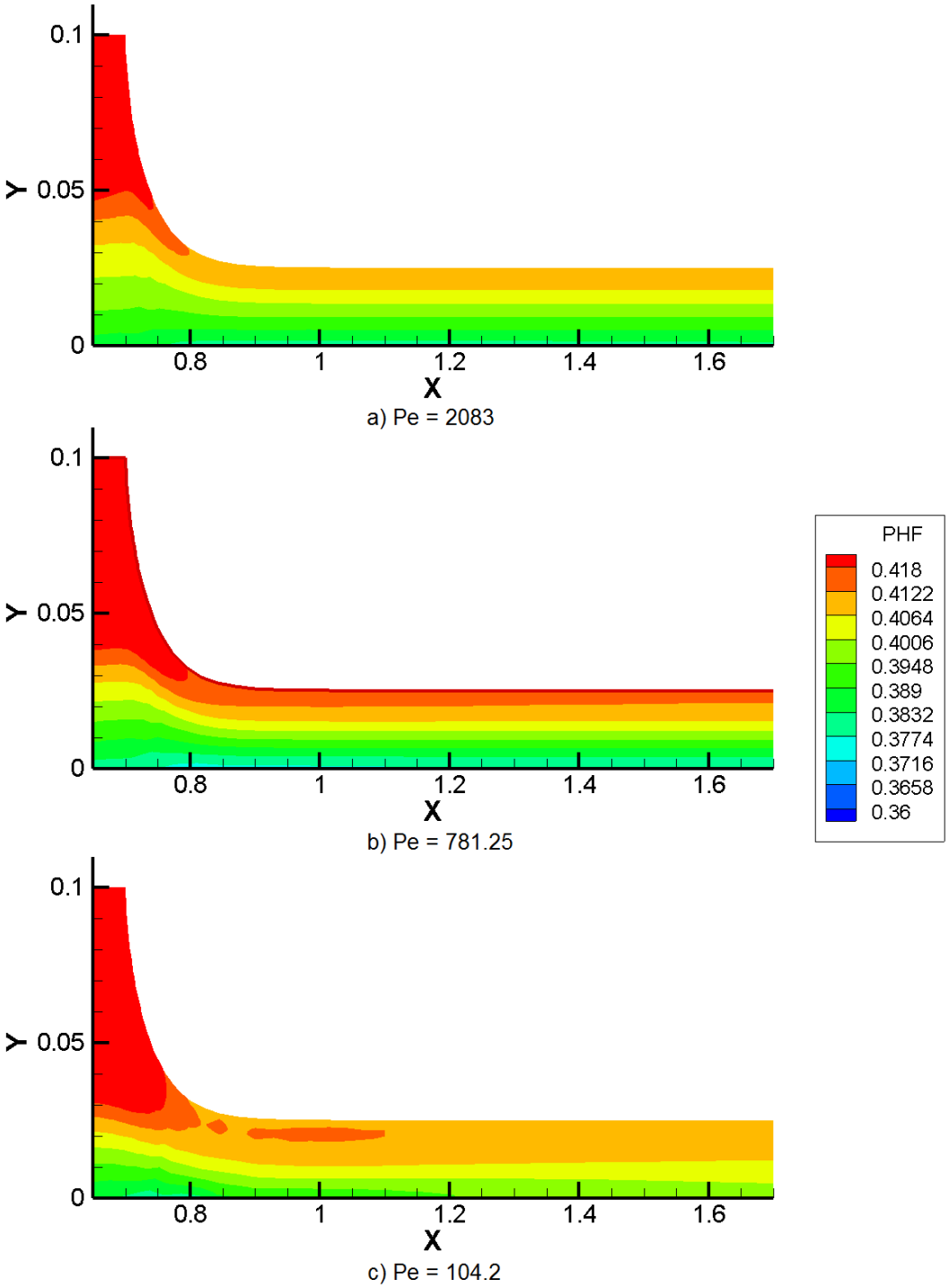

Figure 5.10: Concentration field at the final region for (a) $Pe = 2083$, (b) $Pe = 781.25$ and (c) $Pe = 104.2$ ($k = 0.4$, $S = 0$, $Ca = 0.05$ and $h = 4$).

distribution along the thickness of the coated layer. This study is discussed in the next subsection.

5.2.2
Effect of $k = K_c/K_\mu$

Figure 5.11 shows the different particle distributions on the coated film as a function of k. As k decreases, K_μ increases and, as a consequence, particle migration due to viscosity gradient mecanism becomes stronger. Therefore, as k falls, particle profile becomes more uniform.

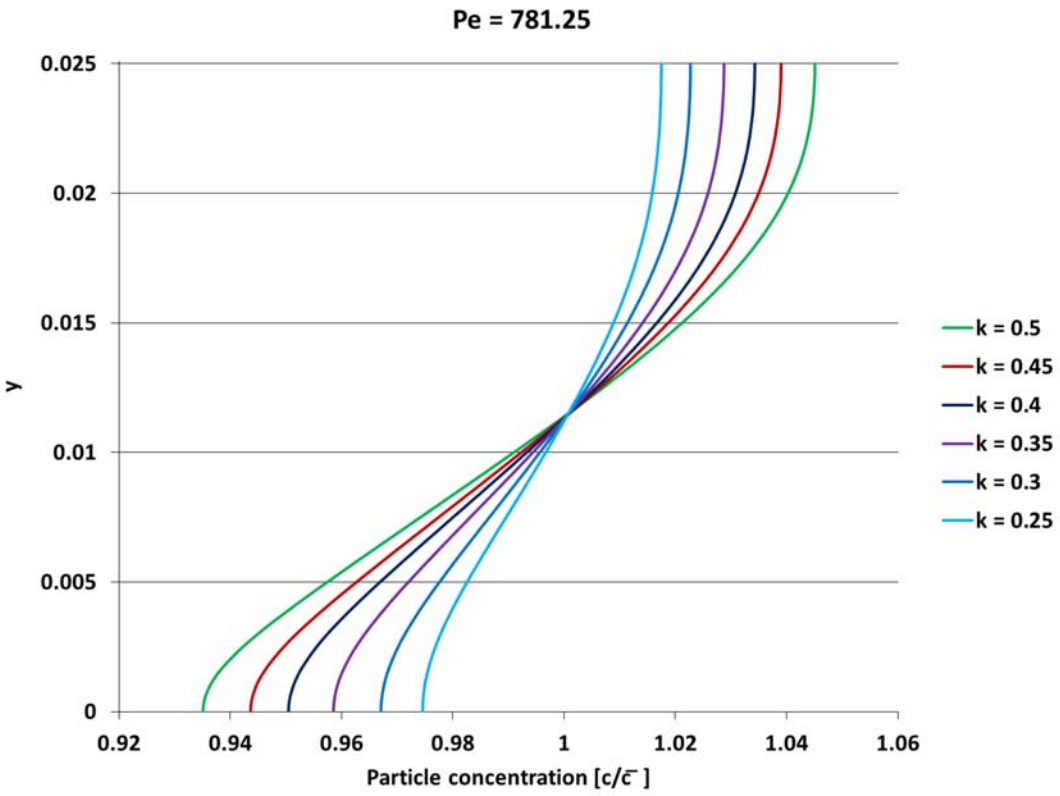

Figure 5.11: Particle profile as a function of k ratio when $Pe = 781.25$ ($S = 0$, $Ca = 0.05$ and $h = 4$).

The same behavior was seen in subsection 5.1.2. Therefore, independent of the final film thickness, as k decreases, particle profile becomes more uniform.

To study sedimentation the two most extreme profiles were used: $k = 0.25$ and $k = 0.5$. As it was explained earlier, Pe will be kept constant and equal to 781.25.

5.2.3
Effect of Particle Sedimentation S

Figures 5.12 and 5.13 show the results for sedimentation effect at $k = 0.25$ and $k = 0.5$, respectively. As density difference between particles and liquid increases, particle concentration increases at the bottom and decreases at the top of the film, for both cases.

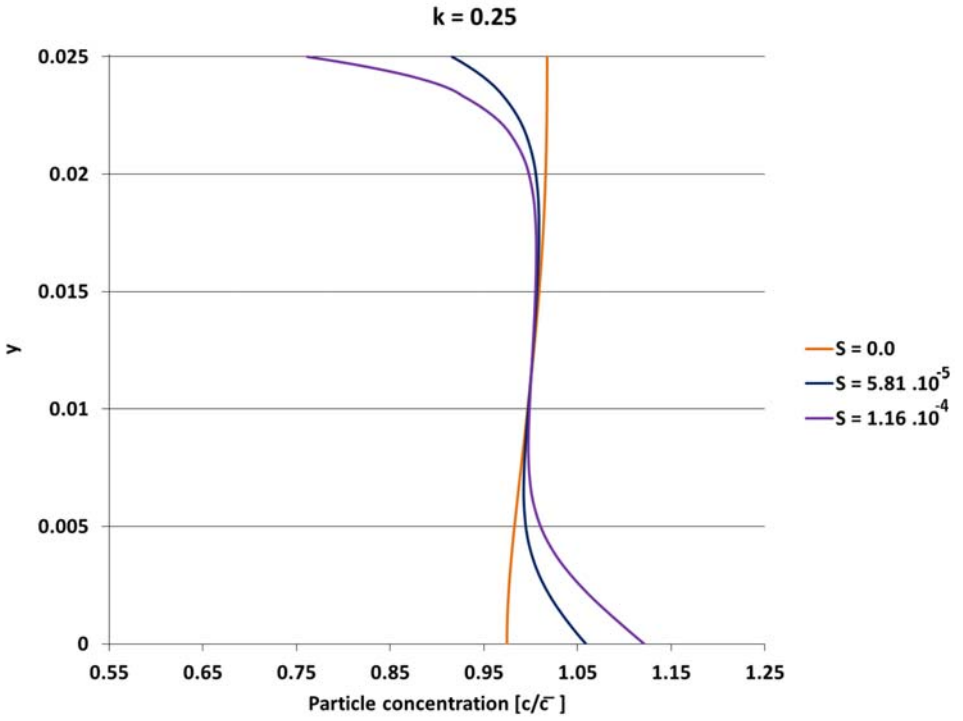

Figure 5.12: Final particle distribution at the coated layer for different density difference between particle and liquid, where $k = 0.25$ ($Pe = 781.25$, $Ca = 0.05$ and $h = 4$).

Figures 5.14 and 5.15 compares particle distribution on the coated layer at a fixed value of S and different values of k. Figure 5.11 shows that $k = 0.5$ yields a more non-uniform particle profile than $k = 0.25$. This was explained by the fact that lower k means higher particle migration due to viscosity gradient and, as a consequence, more uniform profile. In figure 5.14, particle profile is indeed more uniform at $k = 0.25$ than at $k = 0.5$. However, as density difference increases, profile at $k = 0.5$ is almost as uniform as $k = 0.25$. Still, $k = 0.5$ yields greater particle concentration difference between the bottom and the top of the film than $k = 0.25$.

Table 5.3 shows sedimentation numbers related to all different density differences used. Once again sedimentation number is really small in all cases. This is why particle profile does not change much in the middle of the film as figures 5.12 and 5.13 shows. Even though convective transport is much stronger than sedimentation, sedimentation was still able to change final particle profile at the top and bottom of the film.

As a conclusion, it is extremely hard to predict final particle distribution based on simple flow models because particle profile may change drastically due to different characteristics of the flow in different regions. From the present work, we may conclude that particle profile is a function of film thickness,

Table 5.3: Values of S parameter for the cases of Figures 5.12 and 5.13.

	$\Delta\rho$ $[g/mm^3]$	S
$k = 0.1$	0	0.0
	1.10^{-3}	$1.16 \cdot 10^{-5}$
	3.10^{-3}	$3.48 \cdot 10^{-5}$
	5.10^{-3}	$5.81 \cdot 10^{-5}$
	8.10^{-3}	$9.29 \cdot 10^{-5}$
	1.10^{-2}	$1.16 \cdot 10^{-4}$

Peclet number, k and sedimentation.

5.3 Marangoni Flow

Up to now, all predictions were for surface-passive particles that have no effect on the liquid surface tension. In this section, we explore the effect of particle concentration on surface tension, which yields surface tension gradients along the interface.

First, we consider that particle migration from the bulk to the interface

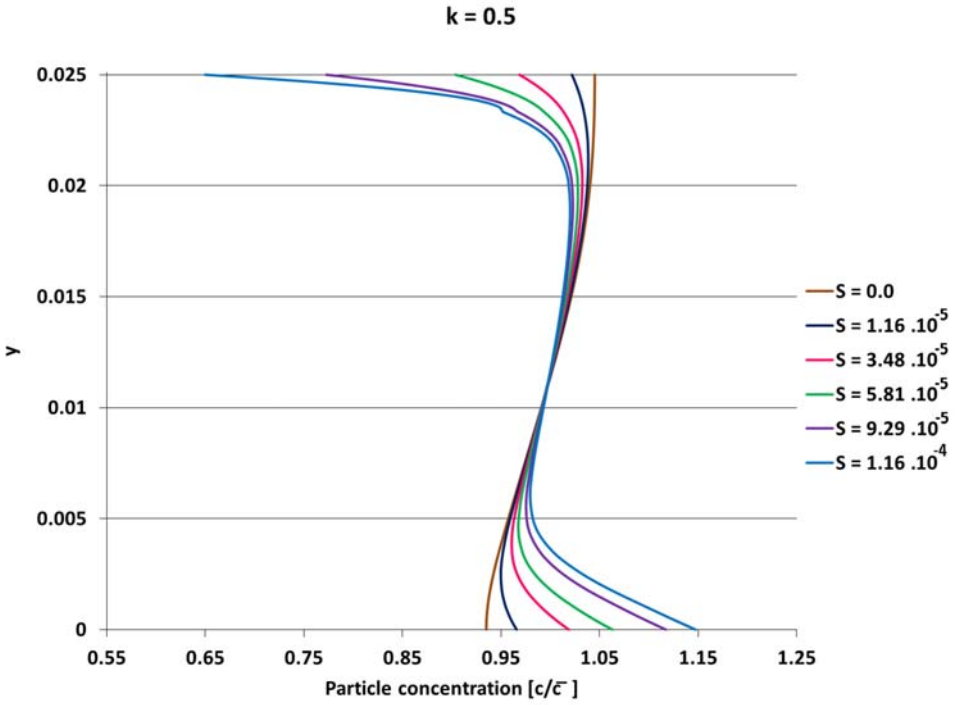

Figure 5.13: Final particle distribution at the coated layer for different density difference between particle and liquid, where $k = 0.5$ ($Pe = 781.25$, $Ca = 0.05$ and $h = 4$).

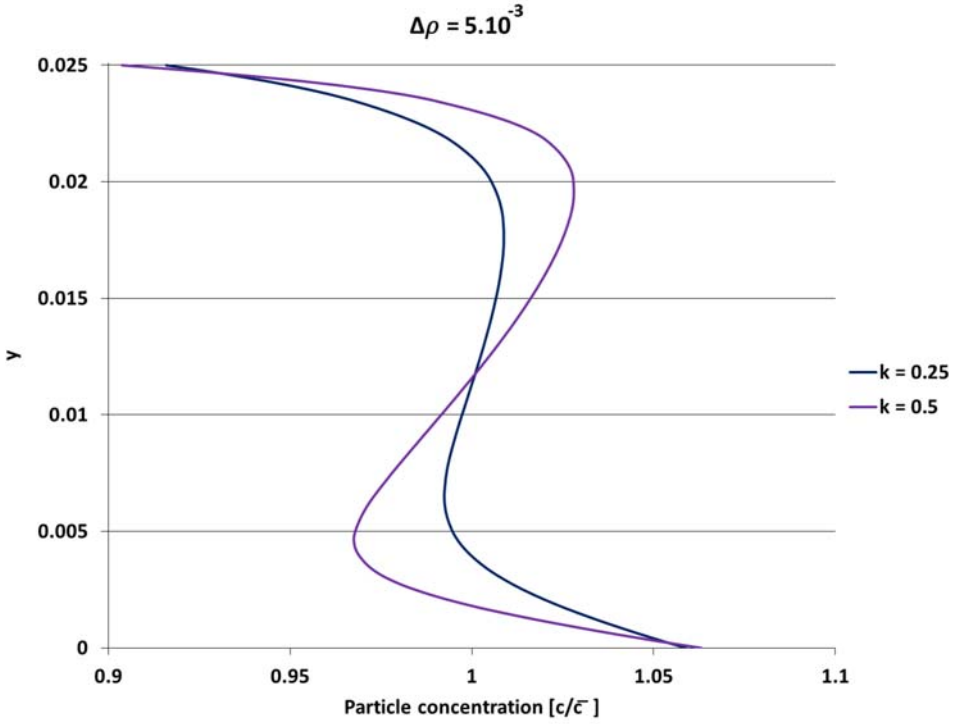

Figure 5.14: Final particle distribution at the coated layer for different density difference between particle and liquid, where $k = 0.25$ ($Pe = 781.25$, $Ca = 0.05$ and $h = 4$).

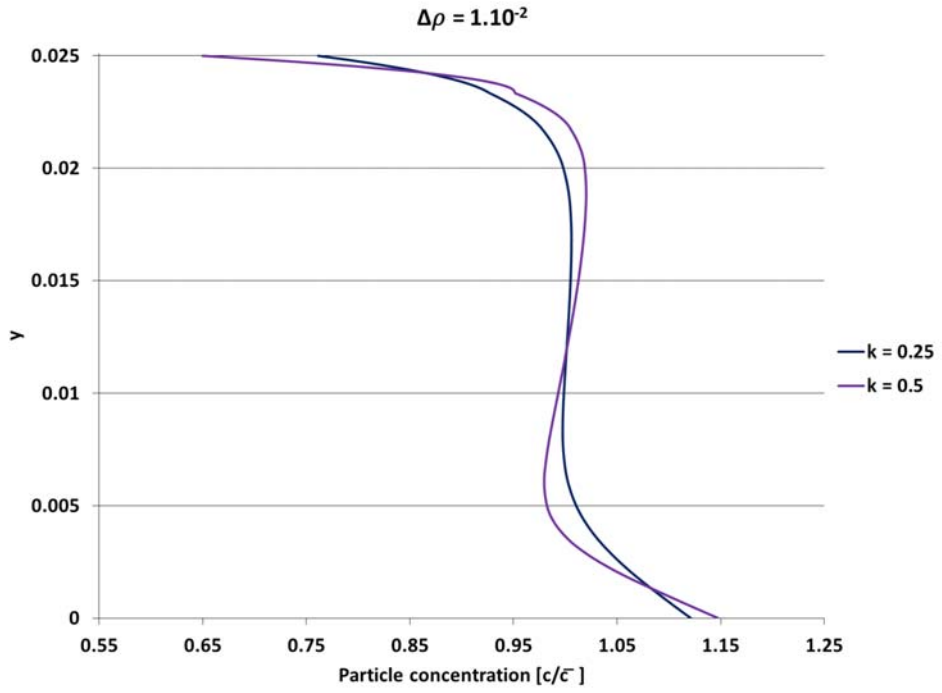

Figure 5.15: Final particle distribution at the coated layer for different density difference between particle and liquid, where $k = 0.5$ ($Pe = 781.25$, $Ca = 0.05$ and $h = 4$).

is instantaneous, hence particle concentration along the interface equals bulk concentration, as it was described in section 2.5. In order to study the marangoni effect, two different cases will be studied from the previous section: one case without sedimentation ($k = 0.25$ and $S = 0.0$) and another with sedimentation ($k = 0.5$ and $S = 5.81 \cdot 10^{-5}$).

As it was defined in section 2.5, surface tension dependency of particle concentration is a function of a parameter β which measures particles strength. Therefore, the parametric analysis is based on β; which will vary from zero to the maximum possible value. This maximum value is determined by model convergence limits due to the high non-linearity of the problem.

Figure 5.16 shows the stream lines and particle concentration field near the downstream free surface for different values of β. The parameters of this flow are: $Pe = 781.25$, $k = 0.25$ and $S = 0.0$. In the first case (figure 5.16(a)), the surface tension is constant. In the second case, surface tension is lower in the high concentration regions.

Marangoni flow led to a more uniform particle concentration along the interface. Figure 5.16(a) shows higher particle concentration gradient along the interface than 5.16(b).

The change on the particle distribution along the interface can be explained by the flow pattern modification caused by surface tension gradient. As β increases, the recirculation under the die lip and near the meniscus changes in such way that shifts the stagnation point towards the contact line. For $\beta = 0$, stagnation point is approximately at $y = 0.065$, and for $\beta = 90$, stagnation point shifts to $y = 0.085$. Without a flow splitting stagnation point in the interface, the particle concentration distribution becomes more uniform. This effect of the surface tension gradient on recirculation pattern near meniscus in coating flow was also reported by Campana and Saita (2006) for the case of dip coating.

Figure 5.17 presents the flow at $Pe = 781.25$, $k = 0.5$ and $S = 5.81 \cdot 10^{-5}$. In figure 5.17(a) there is no effect on surface tension by particle concentration ($\beta = 0.0$), and in figure 5.17(b) surface tension changes with particle concentration ($\beta = 17.0$). When there is no sedimentation, higher values of β were achieved; however with sedimentation the non-linearity of the problem yields results for a lower limit of β.

Even though less intense than figure 5.16, figure 5.17 also shows that particle concentration is smoothed along the interface and stagnation point is shifted due to marangoni flow.

Since surface tension is not constant along the interface, the force balance may lead to changes in the local curvature of the meniscus. Figures 5.18(a) and

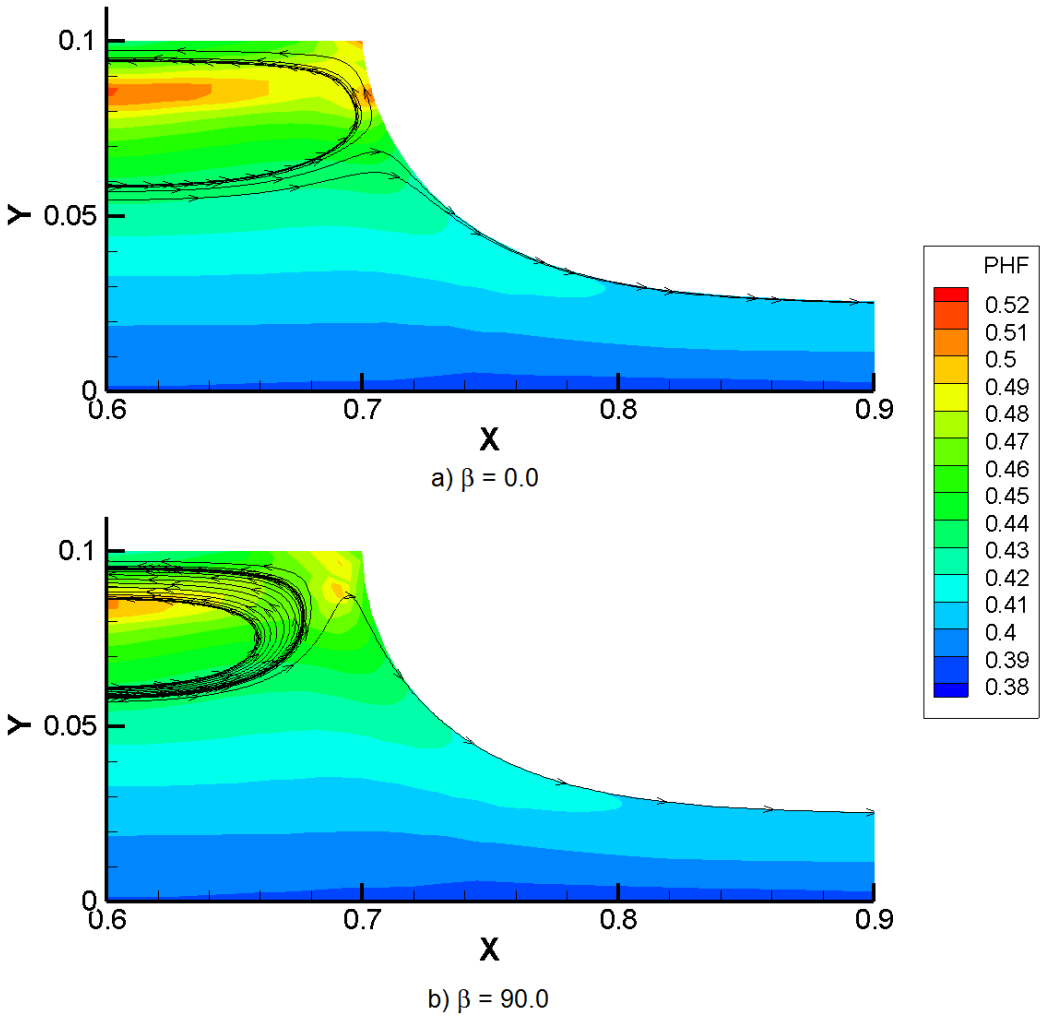

Figure 5.16: Flow at downstream region closer to free surface for (a) $\beta = 0.0$ and (b) $\beta = 90.0$ ($Pe = 781.25$, $k = 0.25$, $S = 0$, $Ca = 0.05$ and $h = 4$).

5.18(b) show the configuration of downstream meniscus for the cases shown in Figures 5.16 and 5.17. In figure 5.18(a), downstream curvature changes a little bit even though β changes a lot. In figure 5.18(b) neither the position nor the curvature of the meniscus changes appreciably.

As a conclusion, surface tension is capable of affecting downstream flow and particle concentration along the interface closer to the downstream region. However it does not change significantly the downstream meniscus. Another important point to discuss is if marangoni contribution affects the final particle distribution at the coated film.

Figures 5.19 and 5.20 show the results for the final particle profile as a function of parameter β for both cases studied. Even though surface tension was able to affect the downstream flow and particle concentration along the surface, it did not change at all particle distribution at the coated layer. Therefore, independently of what happened closer to downstream free

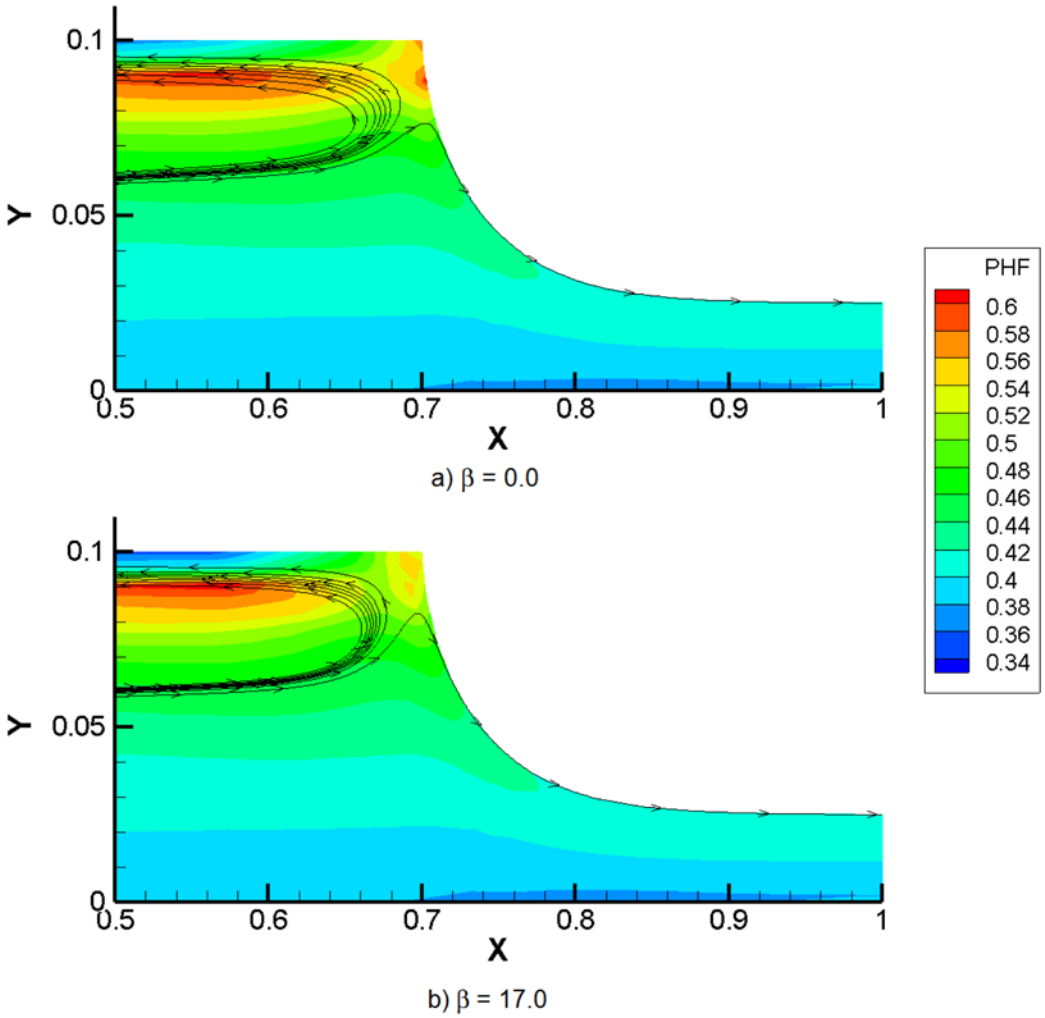

Figure 5.17: Flow at downstream region closer to free surface for (a) $\beta = 0.0$ and (b) $\beta = 17.0$ ($Pe = 781.25$, $k = 0.5$, $S = 5.81 \cdot 10^{-5}$, $Ca = 0.05$ and $h = 4$).

surface, particles have enough time to re-arrange themselves to yield the same concentration profile obtained for the cases with constant surface tension. This conclusion may not be the same at high Peclet number, at which the diffusion mecanisms are weaker and the particle redistribution in the film is not so strong.

This analysis does not consider particle migration from/towards the interface. Particle migration from the bulk to the interface and vice-versa might change final particle distribution. This will be studied in next section.

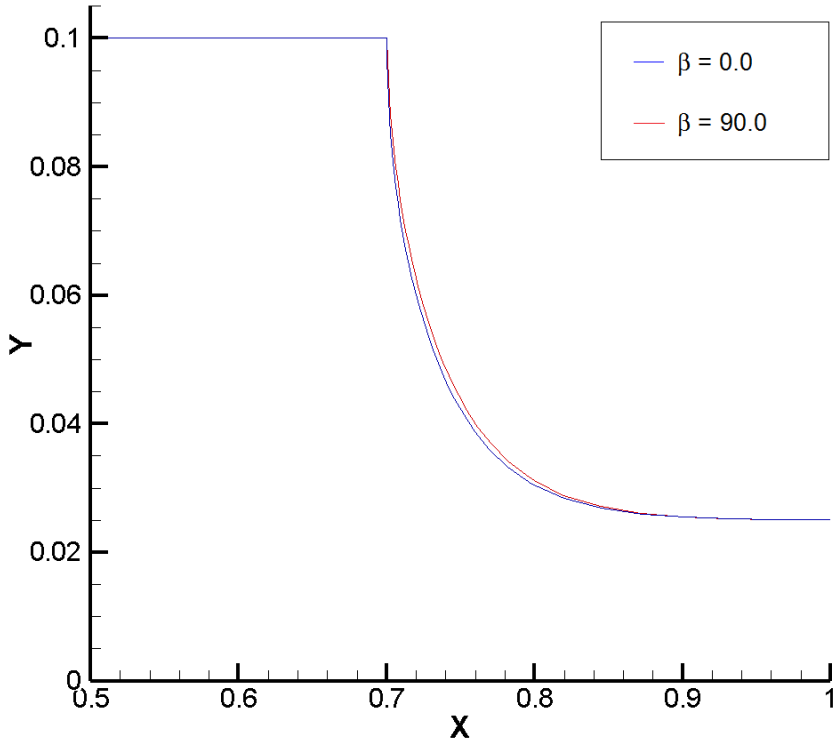

a) k = 0.25 and $\Delta\rho = 0.0$

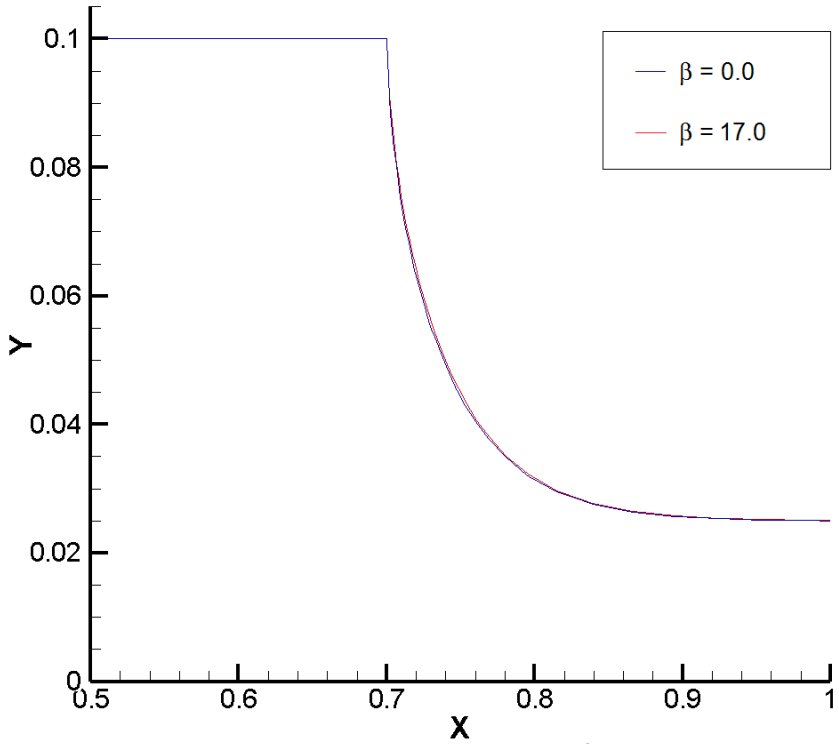

b) k = 0.50 and $\Delta\rho = 5.10^{-3}$

Figure 5.18: Downstream curvature for different values of β in different configurations ($Pe = 781.25$, $Ca = 0.05$ and $h = 4$).

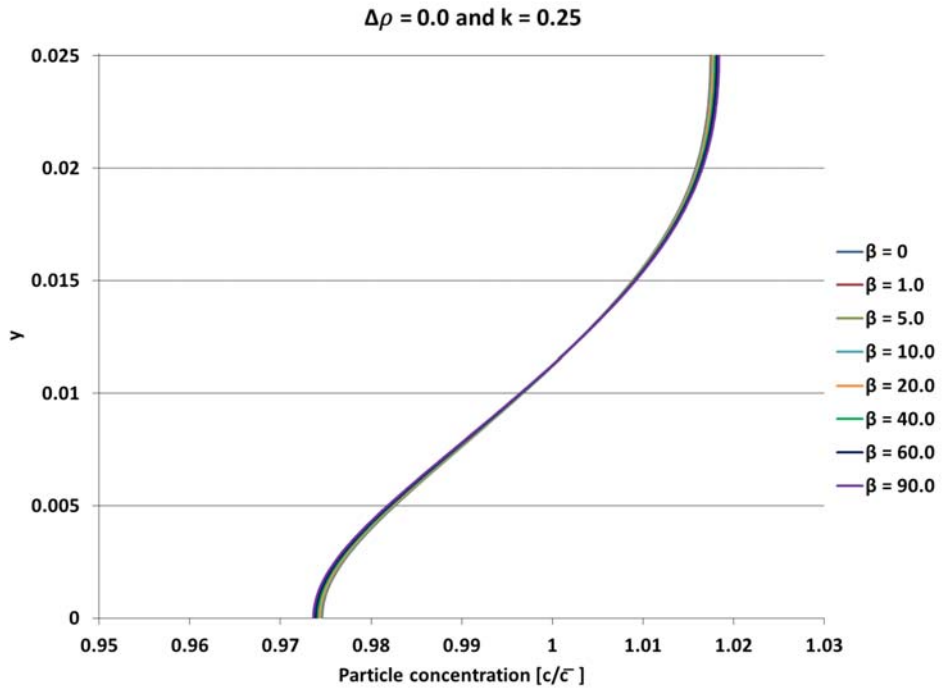

Figure 5.19: Final particle distribution for several values of β ($Pe = 781.25$, $k = 0.25$, $S = 0$, $Ca = 0.05$ and $h = 4$).

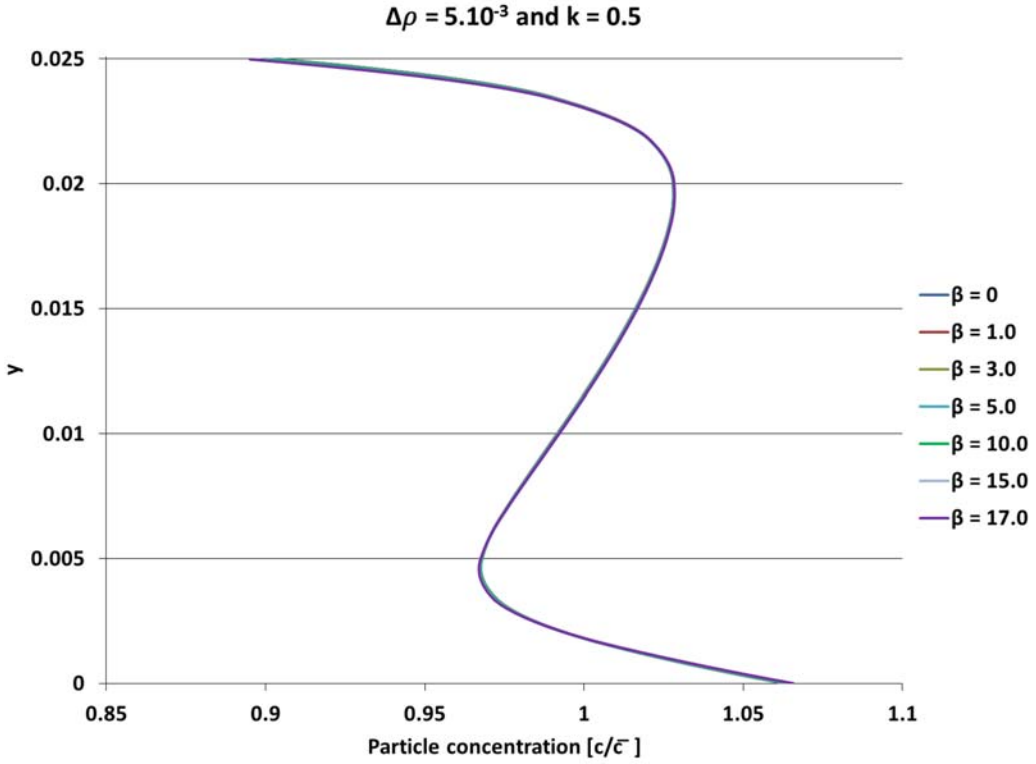

Figure 5.20: Final particle distribution for several values of β ($Pe = 781.25$, $k = 0.5$, $S = 5.81 \cdot 10^{-5}$, $Ca = 0.05$ and $h = 4$).

5.4 Marangoni Flow with Particle Migration to the Interface

In order to evaluate particle concentration along the interface, a one-dimensional element was included in the formulation, as explained in Chapter 3. Now there are three parameters to be studied: k_a (or $S_t = k_a/V$), k_d and β. As it has been done so far, other dimentionless parameters will have a constant values that are: $Pe = 781.25$, $k = 0.25$ and $S = 0.0$. As the parameters to be studied are S_t and β, k_d will be kept constant and equal to 1.0.

First, we analyse particle concentration along the interface and at the region closer to the interface for different values of S_t. The results from an analysis with a constant $\beta = 9.0$ is presented in figure 5.21. In figure 5.21(a), $S_t = 1 \cdot 10^{-5}$, surface concentration is practically zero along all interface. As S_t increases, which means that particle adsorption effect increases, particle concentration at the bulk tends to particle concentration along the interface. As k_d is kept constant and is higher than k_a in both cases, particles concentration along the interface decreases along the x direction.

Now, we analyse the effect of S_t on the flow. Again, β is kept constant and equal to $\beta = 9.0$. Figure 5.22 shows the configuration of the downstream free surface for different values of S_t. The curvature of the interface changes as a function of S_t. As S_t increases, the meniscus becomes more curved and the radius of curvature falls. Besides, as k_a increases, more particle are absorbed by the interface; which, as a consequence, decreases surface tension. Finally, as surface tension falls the meniscus need to curve more in order to satisfy the force balance along the interface.

On the other hand, in figure 5.22, the changes in meniscus curvature are very small and is hard to identify the different curves. That happens because the value of β used is too small to greatly impact the surface tension. However, in the previous section a higher value of β yields a even smaller difference in curvature. To better analyse this effect, one solution is to increase β, however for higher S_t values such as $S_t = 8 \cdot 10^{-3}$ the model does not converge for $\beta > 9.2$. Therefore, we analyzed the influence of β for a small S_t.

Figure 5.23 shows the meniscus configuration for different values of β at $S_t = 1 \cdot 10^{-5}$. Even though S_t is quite small, there is a significant change on the curvature as β increases. For the same range of β, the analysis which adsorption and desorption effects are considered gives a greater difference on the curvature than the analysis which surface concentration equals bulk concentration (figure 5.18).

Finally, both parameters S_t and β affect downstream free surface curvature. And, as a consequence, should affect the process limits and it should be

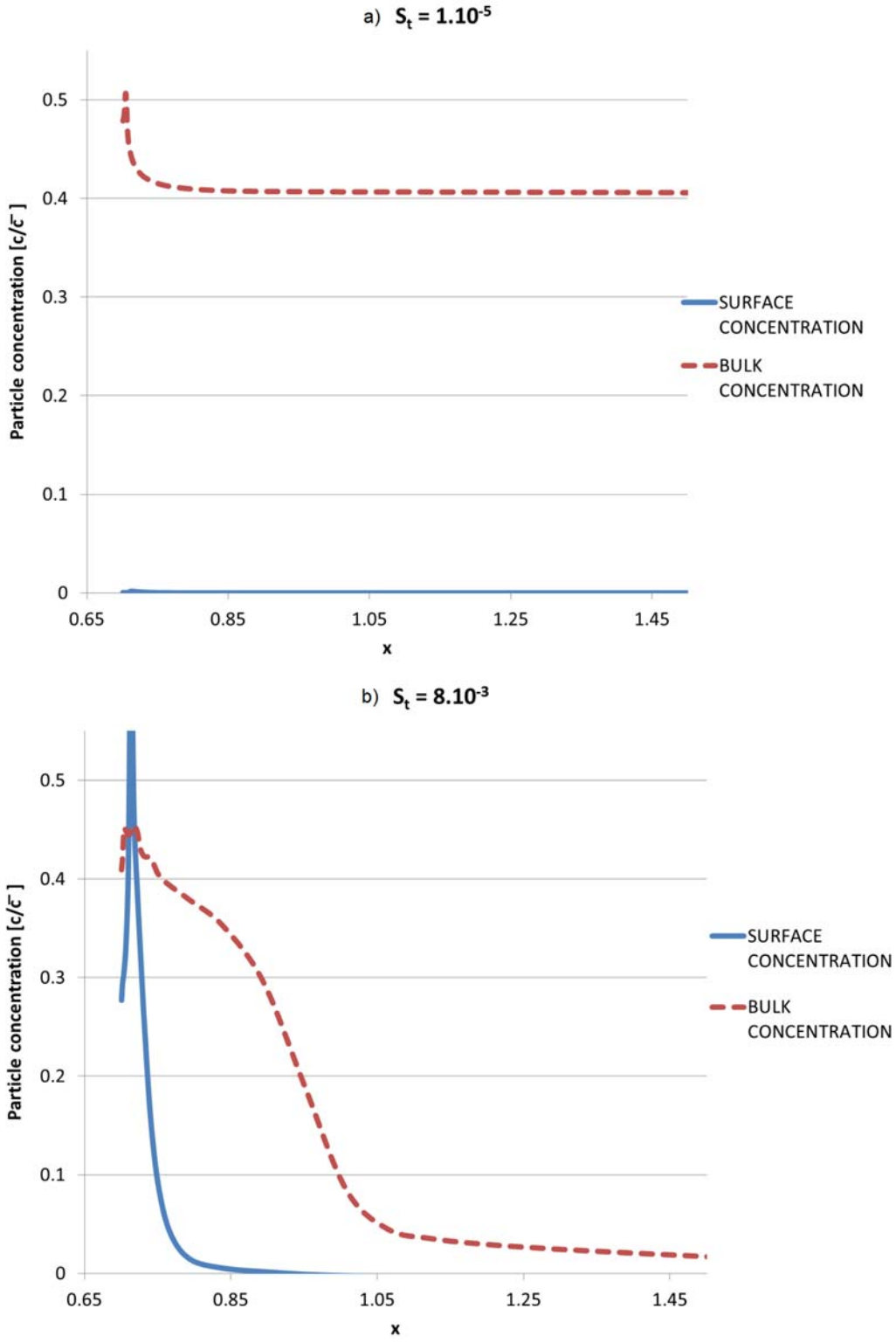

Figure 5.21: Surface and bulk particle concentration for different values of S_t ($Pe = 781.25$, $k = 0.25$, $S = 0.0$, $Ca = 0.05$ and $h = 4$).

taken into account while modeling a coating process.

Section 5.3 showed that evaluate surface tension for a instantaneous particle migration from the bulk to the interface is able to change downstream

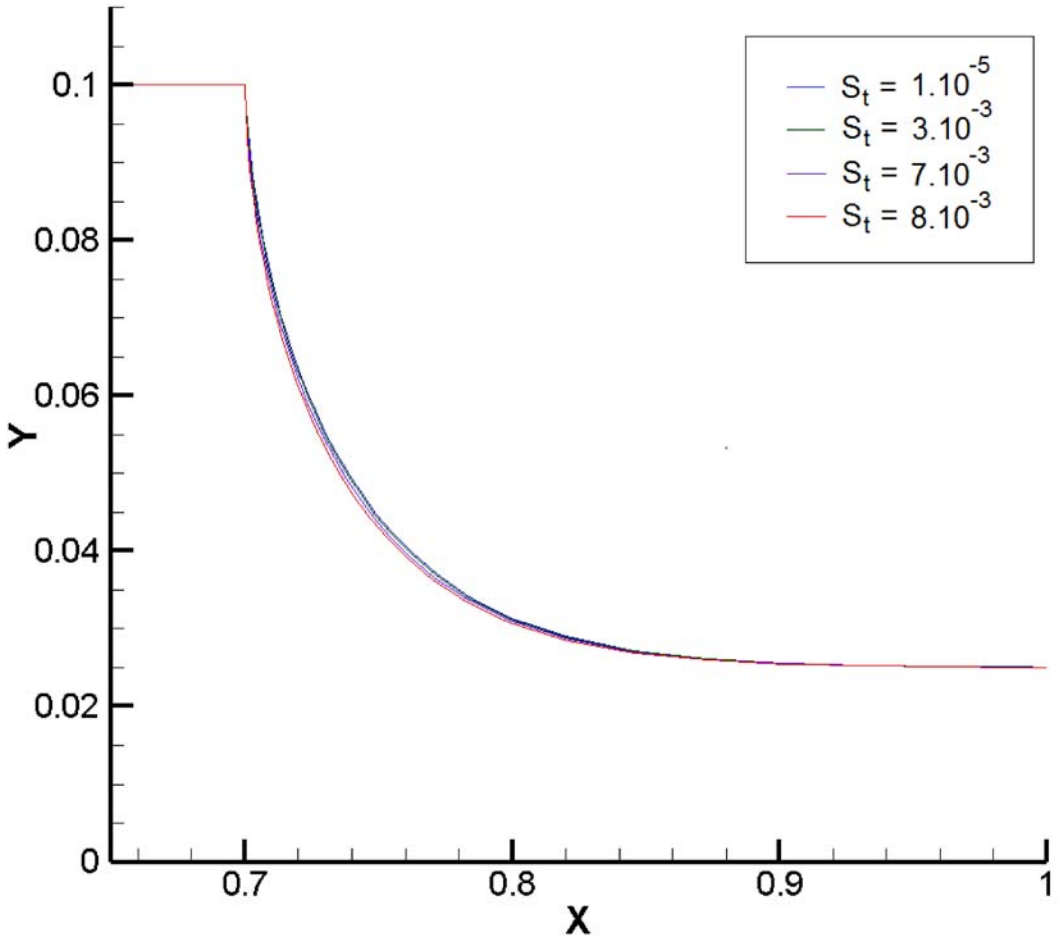

Figure 5.22: Downstream curvature for different values of S_t when $\beta = 9.0$ ($Pe = 781.25$, $k = 0.25$, $S = 0.0$, $Ca = 0.05$ and $h = 4$).

flow but it did not change final particle distribution. Figure 5.24 shows that considering that there is particle migration from the bulk to the interface, marangoni effect may change final particle distribution drastically. As S_t increases, particle concentration in the region closer to the interface decreases. In the rest of the film, particle concentration is practically constant.

Therefore, if adsorption effect is strong enough, particles closer to the interface will be adsorb by the interface and the area just beneath the surface - or the sub-surface area - will have its particle concentration reduced. In order to understand the evolution of this final outcome the concentration field near the downstream meniscus is presented in figure 5.25. In this figure, particle concentration along the interface is not shown, only bulk particle field. Figure 5.25 presents concentration profile for the extreme cases where $S_t = 1 \cdot 10^{-5}$ and $S_t = 8 \cdot 10^{-3}$. As it can be seen, concentration profile along almost all downstream region is the same in both cases; however, closer to the interface particle concentration distribution changes. Essentially, particle concentration in the sub-surface area decreases from case $S_t = 1 \cdot 10^{-5}$ to case $S_t = 8 \cdot 10^{-3}$.

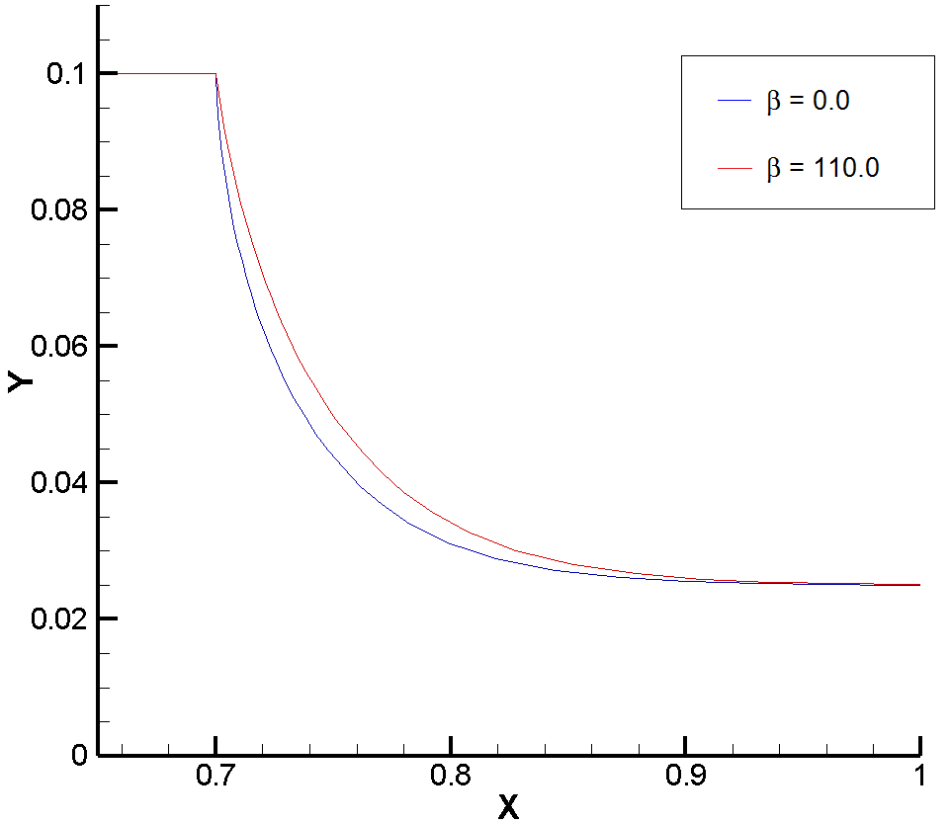

Figure 5.23: Downstream curvature for different values of β when $S_t = 1 \cdot 10^{-5}$ ($Pe = 781.25$, $k = 0.25$, $S = 0.0$, $Ca = 0.05$ and $h = 4$).

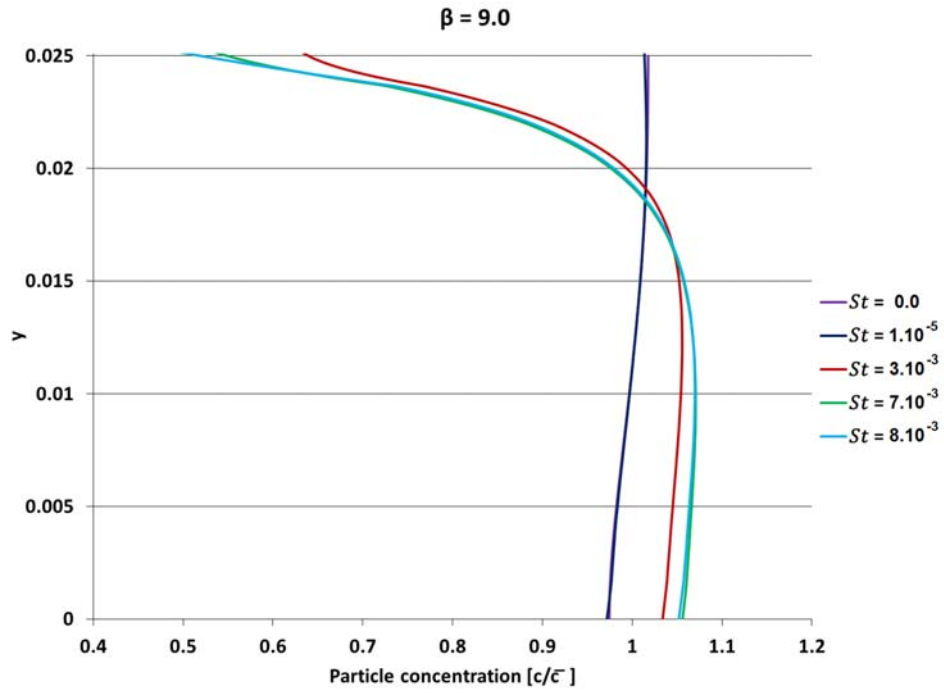

Figure 5.24: Final particle distribution as a function of S_t when $\beta = 9.0$ ($Pe = 781.25$, $k = 0.25$, $S = 0.0$, $Ca = 0.05$ and $h = 4$).

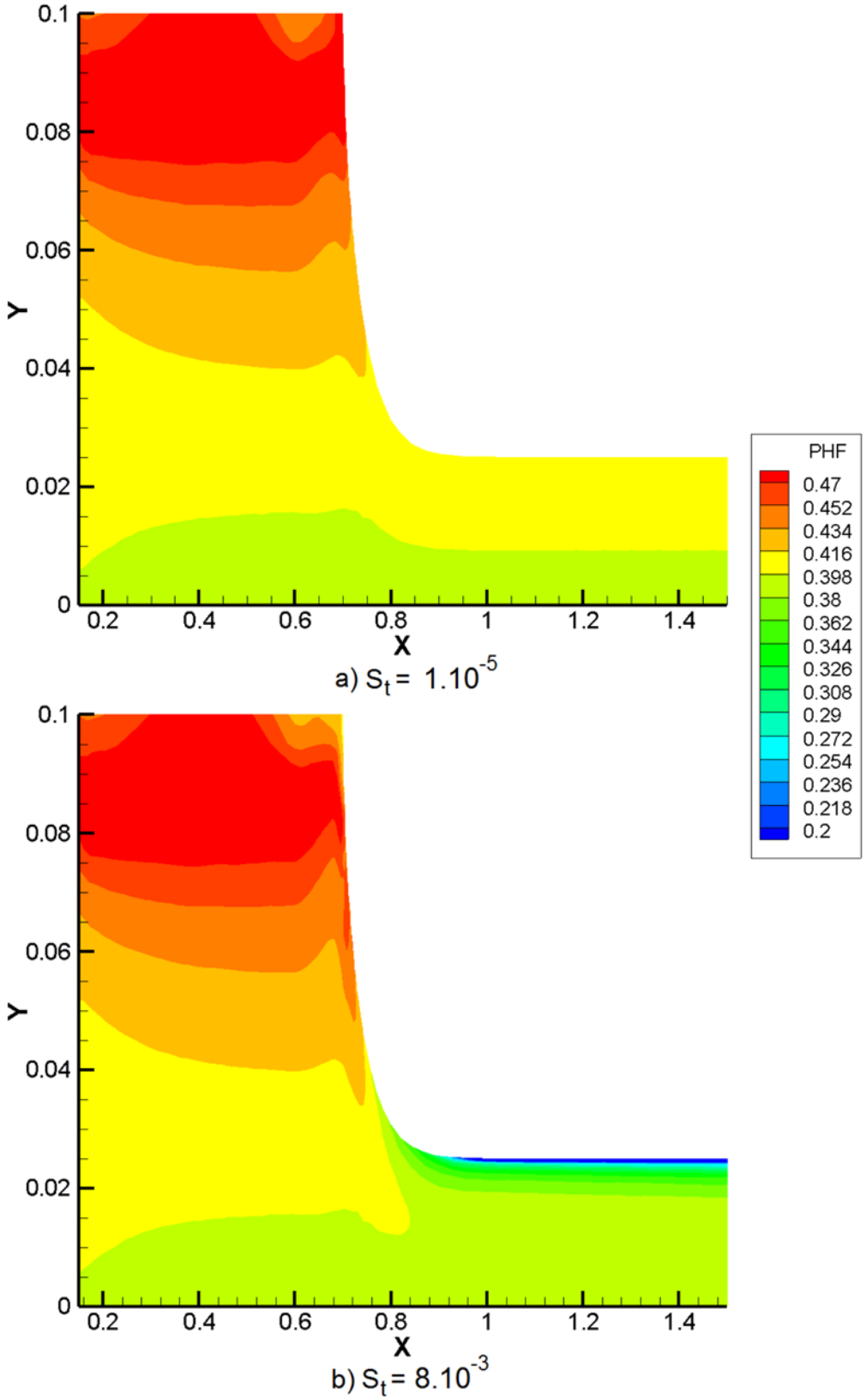

Figure 5.25: Particle concentration field for (a) $S_t = 1{\cdot}10^{-5}$ and (b) $S_t = 8{\cdot}10^{-3}$ ($Pe = 781.25$, $k = 0.25$, $S = 0.0$, $Ca = 0.05$ and $h = 4$).

The final region in figure 5.25(b) shows the evolution of particle distribution. The final result agrees with particle profile presented in figure 5.24. Particle concentration is extremely low in the sub-surface area, and the area far from the interface particle concentration is practically constant.

As it has been presented, the hypothesis that particle concentration along the interface is the same as bulk concentration may not describe correctly particle distribution depending on surface properties. For instance, for $S_t = 1 \cdot 10^{-5}$ final particle distribution did not change as much as $S_t = 8 \cdot 10^{-3}$ case. On the other hand, evaluating particle migration from the bulk to the interface and vice-versa does affect downstream meniscus curvature, even for a case where $S_t = 1 \cdot 10^{-5}$ (figure 5.23), and, as a consequence, process limits.

6
Final Remarks

This Chapter presents the conclusions achieved in the present work. Some limitations of the model presented could be expanded so more accurate results and other analysis were drawn. Those sugestions for future work are also presented in this Chapter, in section 6.2.

6.1
Conclusions

The goal of this work was to propose a model that is able to describe coating process of particle suspension and particularly study how particle distribute themselves in this process as a function of different particle migration mechanisms. In addition, the effect of surface tension gradients due to concentration variation was also studied. The Galerkin Finite Element method and Newton's method were used to solve the non-linear system of partial differential equations. For bulk flow, two-dimensional element was used. Besides, in order to evaluate particle concentration along the interface, one-dimensional element was created along the interface. The present work also presented a way to couple these two elements to study cases that considers particle adsorption and desorption from the interface, and it was succesfully implemented.

There were two main analysis presented in Chapter 5. In section 5.1 particle distribution was studied for a film thickness that is half of the gap. In section 5.2, the results for a film thickness that is one forth of the gap were presented. For both cases, a parametric analysis was performed. The conclusions from the analysis of Pe, k and S at $h = 2$ are presented in Table 6.1. Table 6.2 presents conclusions for same parameters at $h = 4$.

Then, marangoni effect was studied, where surface tension was evaluated as a function of interface concentration. A first simplified model considers that surface concentration is equal bulk concentration. A second, more accurate, model takes into account particle migration towards and away from the interface. The results from the first model show that surface tension gradient does change the flow under the downstream die and shifts stagnation point closer to the die surface. In addition, as surface tension variation with particle

Table 6.1: Conclusions drawn from dimentionless parameters when $h = 2$.

Parameter	$h = 2$
Pe	High Pe ($Pe > 260.4$) yields higher particle concentration in the center of the film. However, low Pe ($Pe \leq 260.4$) yields higher particle concentration at the top of the film.
k	As k decreases particle concentration along the final film thickness becomes more uniform. k behaves monotonically.
S	Even though S is very small, particle concentration at the top of the film decreased, while concentration at the bottom increased as S increases.

Table 6.2: Conclusions drawn from dimentionless parameters when $h = 4$.

Parameter	$h = 4$
Pe	For $2083 < Pe < 781.25$, as Pe decreases particle profile becomes less uniform. When Pe reaches 781.25 this behavior changes. For $Pe < 781.25$, as Pe decreases particle profile becomes more uniform.
k	Similar to case where $h = 2$; as k decreases particle profile becomes more uniform.
S	Similar conclusion to the case where $h = 2$; settling velocity was much slower than web speed for all cases studied. Still, as S increases particle concentration decreases at the top of the film, and increases at the bottom. Also, for higher value of S ($S = 1.16 \cdot 10^{-4}$) particle profile presented similar behavior for different k's.

concentration becomes stronger (β increases), the induced marangoni effect smooths particle concentration along the interface. On the other hand, final particle distribution did not change when adsorption and desorption effects along the interface were not considered; particle profile at the coated film was the same for cases where $\beta = 0.0$ and $\beta = 90.0$.

Finally, particle migration from the bulk to the interface and vice-versa was implemented. As the dimentionless parameter S_t increases, more particles are absorded by the interface, which afects surface tension and, as a consequence, the interface curvature. For a given S_t, different values of β yield different meniscus configuration.

It was found that surface tension, evaluated as a function of surface

particle concentration when adsorption and desorption effects are considered, strongly afects the flow and final particle profile. The case studied presented a uniform particle distribution along the film thickness at $S_t = 0.0$; as S_t increases to $8{\cdot}10^{-3}$, particles migrate to the interface and particle concentration in the sub-surface area decreases while in the rest of the film particles are still uniformly distributed.

As a conclusion, the model proposed is able to describe coating process of particle suspension. In order to determine concentration field, different diffusive mechanisms were used to describe particles migration. The model also includes surface tension variation due to particle concentration, Marangoni flow, which changes recirculation pattern flow, particle distribution and meniscus configuration. Moreover, results drawn from the analysis of surface tension as a function of bulk concentration were quite different from those when particle migration from the bulk to the interface was considered. Therefore, to model coating processes it is important to evaluate interface concentration and its adsorption and desorption effects, because capillary forces are important in such processes and might change process limits. However, the model still has some limitations. Some suggestions for future work are presented in the next section.

6.2 Future work

As mentioned earlier, the model considered that liquid viscosity vary with particle concentration, however it is not a function of shear rate. An important contribution is to include non-Newtonian behavior, as most suspension exhibits shear thinning behavior.

Another point is to consider Brownian diffusion in the equation for particle transport. The present work neglects this mecanism as it considers that particles are big enough that Brownian diffusion is not important. Considering also Brownian diffusion as a possible migration mechanism would yield more accurate results for a wider range of particles diameter.

Results presented in this work showed that surface tension variation affects downstream meniscus curvature. An important study is to analyse quantitatively the effect of particle suspension on the process limits, and how would this affect the coating window.

Coating flow is non-linear and as new parameters and mecanisms are added to the model, it becomes harder to find a solution. Improve numerical method would make possible to study the parameters defined for a wider range of values.

Moreover, there are no experiments in the literature for coating process of particle suspension. Experiments that measures particle distribution in a slot coating process would verify the results obtained from simulation. Besides, migration mecanisms could be better understood and, as a consequence, the coating process.

Finally, expand the model to include drying would help to analyse and understand the effect of final particle distribution on the final product.

Bibliography

[Apostolou and Hrymak (2008)] APOSTOLOU, K.; HRYMAK, A. N. Discrete element simulation of liquid-particle flows. **Computers & Chemical Engineering**, v.32, p. 841–856, 2008.

[Campana and Saita (2006)] CAMPANA, D. M.; SAITA, F. A. Numerical analysis of the rayleigh instability in capillary tubes: The influence of surfactant solubility. **American Institute of Physics**, v.18, n.022104, 2006.

[Carvalho and Kheshgi (2000)] CARVALHO, M. S.; KHESHGI, H. S. Low-flow limit in slot coating: Theory and experiments. **AIChE Journal**, v.46, n.10, p. 1907–1917, 2000.

[Cardinal et al. (2010)] CARDINAL, C. M.; JUNG, Y. D.; AHN, K. H. ; FRANCIS, L. F. Drying regime maps for particulate coatings. **American Institute of Chemical Engineers**, v.56, n.11, p. 2769–2780, 2010.

[Cohen and Guroff (1992)] COHEN, E.; GUTOFF, E. **Modern Coating and Drying Technology**. VCH Publisher, 1992.

[Gadala-Maria and Acrivos (1980)] GADALA-MARIA, F.; ACRIVOS, A. Shear-induced structure in a concentrated suspension of solid spheres. **Journal of Rheology**, v.24, n.6, p. 799–814, 1980.

[Gresho and Sani (2000)] GRESHO, P. M.; SANI, R. L. **Incompressible Flow and the Finite Element Method**. John Wiley & Sons Ltd, 2000.

[Higgins and Scriven (1979)] HIGGINS, B. G.; SCRIVEN, L. E. Capillary pressure and viscous pressure drop set bounds on coating bead operability. **Chemical Engineering Science**, v.35, p. 673–682, 1979.

[Kistler and Schweizer (1997)] KISTLER, S. F.; SCHWEIZER, P. M. **Liquid Film Coating**. first. ed., Chapman & Hall, 1997.

[Krieger (1992)] KRIEGER, I. M. Rheology of monodisperse latices. **Advances in Colloid and Interface Science**, v.3, p. 111–136, 1972.

[Larson (1999)] LARSON, R. G. **The Structure and Rheology of Complex Fluids**. first. ed., Oxford University Press, 1999.

[Leighton and Acrivos (1987)] LEIGHTON, D.; ACRIVOS, A. The shear-induced migration of particles in concentrated suspensions. **Journal of Fluid Mechanics**, v.181, p. 415–439, 1987.

[Min and Kim (2010)] MIN, K. H.; KIM, C. Simulation of particle migration in free-surface flows. **American Institute of Chemical Engineers**, v.56, n.10, p. 2539–2550, 2010.

[Miskin et al. (1996)] MISKIN, I.; ELLIOTT, L.; INGHAM, D. B. ; HAMMOND, P. S. The viscous resuspension of particles in an inclined rectangular fracture. **International Journal of Multiphase Flow**, v.22, n.2, p. 403–415, 1996.

[Okubo (1995)] OKUBO, T. Surface tension of structured colloidal suspensions of polystyrene and silica spheres at the air-water interface. **Journal of Colloid and Interface Science**, v.171, p. 55–62, 1995.

[Panton (2005)] PANTON, R. L. **Incompressible Flow**. third. ed., John Wiley & Sons, 2005.

[Phillips et al. (1992)] PHILLIPS, R. J.; ARMSTRONG, R. C.; BROWN, R. A.; GRAHAM, A. L. ; ABBOTT, J. R. A constitutive equation for concentrated suspensions that accounts for shear-induced particle migration. **American Institute of Physics**, v.4, n.1, p. 30–40, 1992.

[Romero et al. (2004)] ROMERO, O. J.; SUSZYNSKI, W. J.; SCRIVEN, L. E. ; CARVALHO, M. S. Low-flow limit in slot coating of dilute solutions of high molecular weight polymer. **Journal of Non-Newtonian Fluid Mechanics**, v.118, p. 137–156, 2004.

[Romero and Carvalho (2008)] ROMERO, O. J.; CARVALHO, M. S. Response of slot coating flows to periodic disturbances. **Chemical Engineering Science**, v.63, p. 2161–2173, 2008.

[Ruschak (1976)] RUSCHAK, K. J. Limiting flow in a pre-metered coating device. **Chemical Engineering Science**, v.31, p. 1057–1060, 1976.

[Schunk and Scriven (1990)] SCHUNK, P. R.; SCRIVEN, L. E. Constitutive equation for modeling mixed extension and shear in polymer solution processing. **Journal of Rheology**, v.34-37, p. 1085–1119, 1990.

[Silva and Carvalho (2013)] SILVA, L. D. V.; CARVALHO, M. S. **Analysis of slot coating process of particle suspensions**, 2013.

[Szady et al. (1995)] SZADY, M.; SALOMON, T.; LIU, A.; BORNSIDE, D.; ARMSTRONG, R. ; BROWN, R. Anewmixed finite element method for viscoelastic flows governed by differential contitutive equations. **Journal of Non-Newtonian Fluid Mechanics**, v.59, p. 215–243, 1995.